Electrochimica Acta 461 (2023) 142640

Contents lists available at ScienceDirect

Electrochimica Acta

journal homepage: www.journals.elsevier.com/electrochimica-acta

Mass transport limitations in concentrated aqueous electrolyte solutions: Theoretical and experimental study of the hydrogen–bromine flow battery electrolyte

Jakub K. Wlodarczyk [a,*], Norman Baltes [b], K. Andreas Friedrich [c,d], Jürgen O. Schumacher [a]

[a] Institute of Computational Physics, Zurich University of Applied Sciences, Technikumstrasse 71, 8400 Winterthur, Switzerland
[b] Fraunhofer Institute for Chemical Technology, Joseph-von-Fraunhofer-Strasse 7, 76327 Pfinztal, Germany
[c] German Aerospace Center (DLR), Institute of Engineering Thermodynamics, Electrochemical Energy Technology, Pfaffenwaldring 38-40, 70569 Stuttgart, Germany
[d] Institute of Building Energetics, Thermal Engineering and Energy Storage (IGTE), University of Stuttgart, Pfaffenwaldring 6, 70569 Stuttgart, Germany

ARTICLE INFO

Keywords:
Concentrated electrolyte
Hydrogen–bromine flow battery
Mass transport
Ultramicroelectrode
Energy storage

ABSTRACT

Modelling and simulation is a powerful tool to support the development of novel flow cells such as electrolysers and flow batteries. Electrolytes employed in such cells often consist of aqueous solutions of highly concentrated solutes at elevated temperatures. Such conditions pose numerous challenges in conventional model parametrisation because of non-ideal behaviour of the electrolytes. The aim of this work is to study mass transport of electroactive species in highly-concentrated media.

We selected the hydrogen–bromine flow battery posolyte, HBr (aq) and Br_2, as an exemplary flow battery electrolyte and we leveraged chronoamperometric techniques involving ultramicroelectrodes to study diffusion and migration of bromide and bromine at high concentration and temperature. We successfully simulated the current densities of HBr/Br_2 redox reactions in solutions up to 8 mol L^{-1} using advanced mass transport theory which agreed well with the results obtained with ultramicroelectrodes.

While uncharged species transport (Br_2) can be credibly modelled using conventional theories such as Fick's law, charged species (Br^-) require special treatment as the diffusion coefficient vary with concentration up to 50 % with respect to the limiting value at infinite dilution. The transport of charged species without added supporting electrolyte occurs via both migration and diffusion and the contribution of migration current may be up to 50 % of the total current. At HBr concentration > 0.6 mol L^{-1} migration appears to be suppressed due to the "self-screening" effect of the electrolyte.

Proper experimental electrolyte characterisation under operating conditions similar to the actual flow cell applications is indispensable to establish predictive models and digital twins of electrochemical devices. Straightforward transfer of concepts known in electro-analytical chemistry to flow cells modelling may lead to erroneous simulations or model overfitting.

1. Introduction

Industrial electrochemical devices such as electrolysers or flow batteries (FBs) have been recently gaining popularity in the light of constantly growing proportion of energy from intermittent in their nature renewable resources [1]. Large-scale, cost-effective, reliable and safe energy storage systems will play a key role in modern electrical grids, helping to level out imbalances of energy demand and supply over the course of hours to days.

Electrochemical energy conversion devices usually operate at elevated temperatures, such as 50 °C, pressures up to 1000 bar and electrolyte concentrations much exceeding 1 mol L^{-1}, often dictated by engineering design targets (e.g. high energy density), rapid reaction kinetics, favourable thermodynamic properties and eventually, investment profitability. Such operating conditions fall far from those usually employed in electro-analytical chemistry, in which one seeks to separate interfering phenomena and reduce experimental uncertainties. An example of such typical conditions are: using the excess of supporting electrolyte, carrying out experiments at ambient temperatures or utilising minuscule active species concentrations (e.g. in the order of mmol L^{-1}) to simplify theoretical interpretation of the results.

* Corresponding author.
E-mail addresses: j.wlod@protonmail.com (J.K. Wlodarczyk), norman.baltes@ict.fraunhofer.de (N. Baltes), andreas.friedrich@dlr.de (K.A. Friedrich), juergen.schumacher@zhaw.ch (J.O. Schumacher).

https://doi.org/10.1016/j.electacta.2023.142640
Received 22 October 2022; Received in revised form 10 April 2023; Accepted 23 May 2023
Available online 27 May 2023

Such laboratory investigations usually render less useful for analysing large devices. Empirical studies are often coupled with mathematical modelling and simulation [2–4] to allow for gaining a better understanding of the underlying mechanisms and to perform extensive analyses such as optimisation or feasibility study, which shorten the time and spare the resources needed for the product-to-market process. Predictive models, however, necessitate not only a careful selection of constitutive equations representing the most relevant phenomena, but also their accurate parametrisation. Most commonly, these parametrisations are derived from empirical studies, sometimes notwithstanding that the data may have been generated under conditions substantially different from those in the actual application in a flow battery, an electrochemical reactor or an electrolyser.

The rate of diffusion in porous electrodes limits the intensity of mass transport of the reacting species and dictates the maximum current density obtained from an electrochemical cell or stack. It is therefore vital to understand how the diffusion process is affected by the actual operating conditions in an electrolyser or a flow battery.

2. Paper scope and organisation

In this paper, we propose for the first time a reliable method of investigating mass transport limitations stemming from the diffusion and migration of species in FB electrolytes, i.e. in a harsh environment of corrosive and concentrated solutions.

The exemplary target electrochemical system within the scope of this paper is the hydrogen–bromine flow battery (HBFB) – a promising, metal-free alternative to the well-established all-vanadium FB system. However, the ideas presented herein are equally applicable to other FBs, reactors and electrolysers.

We devote our paper to the measurement of the limiting currents due to the redox reactions of the two electroactive species in the actual posolyte of the HBFB [5–7]: the bromide ion (Br^-) and dissolved bromine (Br_2). We investigate the electrolyte at the concentration of up to ca. 8.8 $\mathrm{mol\,L^{-1}}$ in HBr and ca. 6.1 $\mathrm{mol\,L^{-1}}$ in Br_2, utilising powerful methods involving ultramicroelectrodes (UMEs) due to their excellent properties of low ohmic drop even without deliberately added supporting electrolyte, rapid establishment of mass transfer-limited current, high sensitivity and small required sample size. We interpret the experimental findings via mathematical models involving the well-established Fick's law and more advanced ion transport theories. We also indicate newly discovered limitations of the common theories based on Fick's law, widely used in the literature on electrochemical systems models. To the best of our knowledge, this is the first contribution investigating mass transport processes in such highly concentrated aqueous electrolytes utilising UMEs, especially in the chemistry of bromine.

This paper is organised as follows. Section 3 introduces basic information about the HBFB system. Background information on diffusion coefficient measurements can be found in Section 4. Sections 5 and 6 contain an overview of UME techniques and theories of mass transport in electrolyte solutions, respectively. Section 7 includes details of the performed UME experiments. Section 8 provides experimental results with theory validation and a discussion, in which we use theories of mass transport by diffusion to explain the observed deviation from limiting laws. We summarise the paper and delineate possible paths of study extensions in Section 9.

3. The hydrogen–bromine flow battery

HBFB is a hybrid FB consisting of two half cells: a gaseous and a liquid one [8]. The negative pole operates on hydrogen gas, fitted with a membrane-electrode assembly which resembles that of a proton-exchange membrane fuel cell. The positive pole contains an aqueous solution of concentrated hydrobromic acid (HBr) and dissolved elemental Br_2. Sometimes, bromine complexing agents are added to lower the vapour pressure of Br_2 and to increase system safety [9,10]. The negative side reaction reads

$$\frac{1}{2}H_2 \rightleftharpoons H^+ + e^- \tag{1}$$

and the positive side reaction is

$$\frac{1}{2}Br_2 + e^- \rightleftharpoons Br^-. \tag{2}$$

It is well known that Reaction (2) is complicated by a parallel homogeneous chemical reaction which forms polybromides, for example tribromide [6,7,11–13]:

$$Br_2 + Br^- \overset{K_3}{\rightleftharpoons} {Br_3}^- \tag{3}$$

which has the following equilibrium constant, K_3:

$$K_3 = \frac{a_{Br_3^-}}{a^F_{Br_2} a^F_{Br^-}} \tag{4}$$

where a_i is the thermodynamic activity of species i, and superscript F stands for free (uncomplexed) species. Moreover, the formation of higher polybromides such as penta- and heptabromides has been shown to take place in the electrolyte [6,7]:

$$2\,Br_2 + Br^- \overset{K_5}{\rightleftharpoons} {Br_5}^- \tag{5}$$

$$3\,Br_2 + Br^- \overset{K_7}{\rightleftharpoons} {Br_7}^-. \tag{6}$$

4. Existing studies

Diffusion coefficients of ionic species in diluted and concentrated electrolytes have been studied by numerous authors already in the early 20th century [14]. In contrast to physical methods, electrochemical methods of the determination of the diffusion coefficient (e.g. chronoamperometry, chronocoulometry, voltammetry and chronopotentiometry) are fast and easy to implement, but limited only to those species which are converted in an electrochemical reaction under mass transport-controlled regime [15].

These methods give a better insight into the transport phenomena inside electrochemical devices (always involving an actual electrode process), but the results are more difficult to compare with those obtained with non-electrochemical methods, in which the diffusing species are present without deliberately added supporting salts [15].

The diffusion process of species within the scope of this paper, Br^- and Br_2, for the application in industrial-scale devices was studied by Stokes [16]. He measured the ambipolar diffusion coefficient of HBr in up to 1-molar and NaBr up to 2.5-molar aqueous solutions (a range of concentrations) using the diaphragm method at 25 °C. Utilising the same method, Klassen et al. [17] determined the ambipolar diffusion coefficients of aqueous HBr, D_{HBr}, (at ca. 0.2 $\mathrm{mol\,L^{-1}}$ in HBr) in highly concentrated H_2SO_4 (30, 60, 72 wt%). D_{HBr} decreased with decreasing temperature and with increasing H_2SO_4 content. The authors explained the second effect by considering high viscosity of H_2SO_4 as the only factor.

Regarding the literature on the electrochemistry of bromine and bromide, Hwang et al. [18] investigated mass transfer of Br species during electrochemical oxidation of bromide in quaternary ammonium bromide (QBr, used as bromine complexing agents in Br-based FB) by employing platinum (Pt) UME. During the formation of QBr droplets due to phase separation of QBr from the aqueous phase, the electric current of Br^- oxidation in cyclic voltammetry (CV) and chronoamperometry (CA) experiments displayed noise spikes due to QBr droplets stochastically colliding with Pt UME surface.

In a study by Chen et al. [19], the diffusion coefficient of Br^-, D_{Br^-}, in a diluted NaBr solution (5 $\mathrm{mmol\,L^{-1}}$) with 0.1 $\mathrm{mol\,L^{-1}}$ HNO_3 of supporting electrolyte was determined using a Pt UME ($D_{Br^-} = 2.1 \cdot$

10^{-9} $m^2\,s^{-1}$) and agreed well with the literature data [20]. It was then used in simulations of an electrochemical reaction followed by a homogeneous chemical reaction, like reactions (2) and (3), respectively. Piatnicki [21] investigated generally mass transport-limited currents at UMEs in the absence of supporting electrolyte — the case very relevant for our current study.

The previous studies focused on diffusive mass transport at a single electrolyte concentration and did not report the impact of broad range of concentrations and temperature on mass transport of species due to an electrochemical reaction.

5. Ultramicroelectrodes as an analytical technique

In this section, we provide an overview of one of the most powerful analytical tools used in modern electrochemistry termed ultramicroelectrodes [22,23]. UMEs are electrodes having at least one dimension (such as the radius of a disc or the width of a band) smaller than 25 μm [24].

In the simplest case for UMEs, the mass transfer can be described by spherical diffusion, according to:

$$\frac{\partial c_i}{\partial t} = D_i\left(\frac{\partial^2 c_i}{\partial r^2} + \frac{2}{r}\frac{\partial c_i}{\partial r}\right) \tag{7}$$

where c_i is the molar concentration of electroactive species i ($mol\,L^{-1}$), D_i their diffusion coefficient ($m^2\,s^{-1}$), t is time (s), and r is the radial spatial coordinate (m).

Assuming a purely diffusive mass transport to/from a stationary UME, it can be shown by solving Eq. (7) that the diffusion-limited current density, i^{d} ($A\,m^{-2}$), at the spherical UME subject to a potential step until the limiting current conditions is a sum of steady-state and transient components [23]:

$$i^{\mathrm{d}} = \frac{nFDc_i^*}{r_{\mathrm{s}}} + \frac{nF\sqrt{D}c_i^*}{\sqrt{\pi t}} \tag{8}$$

where n is the number of electrons transferred, F is the Faraday constant (96 485 $C\,mol^{-1}$), r_{s} is the electrode (sphere) radius and the asterisk indicates bulk concentration.

The first term due to the spherical diffusion dominates for longer times and the steady state is obtained, in which the current density depends on the size of the electrode. For a UME of r_s = 2.5 μm, the steady state is typically reached after 4 s [23].

It can be shown from Eq. (8) that the steady-state current from a UME, $I_{\mathrm{lim}}^{\mathrm{d}}$ (A) is [22]:

$$I_{\mathrm{lim}}^{\mathrm{d}} = anFD_ic_i^* \tag{9}$$

where a is the geometry factor, $a = 4\pi r_{\mathrm{s}}$ for a spherical electrode and $a = 4r_0$ for a microdisc of radius r_0.

Due to their small size comparable to the diffusion layer thickness, the mass transfer rate by diffusion at a *stationary* UME is comparable to the mass transport at a rotating disc electrode (RDE) operating at *thousands* of revolutions per minute [22].

6. Modelling of diffusion in electrolyte solutions

6.1. Infinitely dilute solutions with excess supporting electrolyte

We consider an ionic aqueous solution consisting of $\nu_- A^{z-}$ anions, $\nu_+ B^{z+}$ cations and water, where ν_i is the stoichiometric coefficient of the ionic species i: anions (–) and cations (+) in the solute chemical formula and z_i is their charge. In a hypothetical limiting case of an infinitely diluted electrolyte, the limiting molar conductivity of a monovalent, binary electrolyte, Λ° ($S\,cm^2\,mol^{-1}$), is:

$$\Lambda^\circ = \nu_+\lambda_+^\circ + \nu_-\lambda_-^\circ \tag{10}$$

where λ_i ($S\,cm^2\,mol^{-1}$) is the molar ionic conductivity of species i.

The (limiting) molar conductivities of species i are closely related to their (limiting) ionic mobilities in the electric field, u_i ($m^2\,s^{-1}\,V^{-1}$) by

$$\lambda_i = |z_i|u_iF. \tag{11}$$

In the electrolyte composed of *small amount* of electroactive ions i and an *excess* of the supporting electrolyte, the electroactive species move through a stagnant solution in a diffusion process [14] which is described by:

$$J_i = -D_i^\circ\frac{\partial c_i}{\partial x} \tag{12}$$

where J_i is the molar flux of electroactive species i ($mol\,s^{-1}\,m^{-2}$), D_i° is the single-ion diffusion coefficient of electroactive species i at infinite dilution in i ($m^2\,s^{-1}$) and x is the spatial coordinate (m). It should be noted that D_i° depends, however, on the concentration of the supporting electrolyte, but not on the concentration of species i in the limit of infinite dilution with respect to i [25].

In the purely diffusive transport, any change in the limiting current at constant temperature will be due to the change of diffusion coefficients of electroactive species with the ionic strength. Even at extremely small concentrations of the diffusing species, the observed diffusion coefficients, $D_i^{\circ\prime}$ are expected to vary linearly [26], [27, p. 298–306] with the square root of the ionic strength, $I_{\mathrm{st}} = 0.5\sum_{i=1}^{N} c_i z_i^2$ ($mol\,L^{-1}$) for N species, as [21]:

$$D_i^{\circ\prime} = D_i^\circ(1 - \alpha\sqrt{I_{\mathrm{st}}}) \tag{13}$$

where α is an empirical constant and D_i° is the (true) limiting diffusion coefficient of i – in the limit of infinite dilution in *both* species i and the supporting electrolyte. It is the D_i° which is reported in the literature as it depends barely on the type of ion and not on its own concentration or the concentration of the supporting salt.

The so-called single-ion diffusion coefficients can be theoretically calculated at infinite dilution using the Nernst–Einstein relation [14,21,28]:

$$D_i^\circ = \frac{\lambda_i^\circ RT}{F^2 z_i^2} \tag{14}$$

where R is the universal gas constant (8.314 $J\,K^{-1}\,mol^{-1}$) and T is the absolute temperature (K).

Eqs. (11), (12) and (14) have been widely adopted in the literature treating fuel cells and flow batteries [29–36]. In such systems, however, the operating conditions rarely correspond to those used in analytical electrochemistry. This fact raises an important question whether the multiphysics electrochemical models can be predictive enough, being based on the equations straightforwardly carried from analytical electrochemistry applications.

Recalling the particular case of HBFB modelling literature, the adopted single-ion diffusion coefficients of bromide used in Eq. (12) are reported to vary from $1.78\cdot10^{-5}$ $cm^2\,s^{-1}$ [29] through $2.08\cdot10^{-5}$ $cm^2\,s^{-1}$ [33,35,36] to even $3.87\cdot10^{-5}$ $cm^2\,s^{-1}$ [37]. In the results section, we shall discuss the applicable value of $D_{\mathrm{Br^-}}^\circ$ for bromine-based HBFB modelling.

6.2. Infinitely diluted solutions without supporting electrolyte

In a diluted, simple and strong electrolyte, the electroneutrality condition:

$$\sum_i z_i c_i = 0 \tag{15}$$

prevents macroscopic charge separation and entails the fact that *without applying an external electric field*, anions and cations diffuse through the solvent effectively as a single component (salt), similarly to the molecular diffusion of neutral species [14,38–40], and not like single

ionic species. The steady-state flux of this salt (s) in water (w) for a binary, diluted aqueous electrolyte may also be described by [14]:

$$J_{sw} = -D^{\circ}_{sw}\frac{\partial c_s}{\partial x} \tag{16}$$

where D°_{sw} ($m^2\,s^{-1}$) is the so-called *ambipolar* ("salt") diffusion coefficient at infinite dilution.

For binary, strong electrolytes, it can be shown [14] that it is possible to calculate D°_{sw} from the single-ion diffusion coefficients of the constitutive ions (or, equivalently, their limiting mobilities or molar conductivities) as follows:

$$\begin{aligned} D^{\circ}_{sw} &= \frac{D^{\circ}_{+}D^{\circ}_{-}(\nu_{+}+\nu_{-})}{\nu_{-}D^{\circ}_{+}+\nu_{+}D^{\circ}_{-}} = \frac{RT}{F}\frac{u^{\circ}_{+}u^{\circ}_{-}(\nu_{+}+\nu_{-})}{\nu_{+}z_{+}(u^{\circ}_{+}+u^{\circ}_{-})} \\ &= \frac{RT}{F^2}\frac{\lambda^{\circ}_{+}\lambda^{\circ}_{-}(\nu_{+}+\nu_{-})}{z_{+}\nu_{+}(\lambda^{\circ}_{+}|z_{-}|+\lambda^{\circ}_{-}z_{+})}. \end{aligned} \tag{17}$$

In this paper, we limit our investigations to binary electrolytes and focus more on the extension of the theory to high concentrations, as for trenary and higher cases, the equations become even more complicated with more coefficients needed to describe the whole system. For three and more ionic species, Eq. (15) may be satisfied in an infinite number of ways and the general equations can be derived, but not necessarily solved [14].

6.3. From infinitely diluted to moderately diluted solutions

Commonly, on increasing electrolyte concentration, the diffusion coefficient of a strong aqueous electrolyte decreases rapidly from the limiting value for infinite dilution [14,26,41], D°_{sw}, similarly to the activity coefficients of electrolytes.

The ambipolar (salt) diffusion coefficient is related to the chemical potential of the solute (salt), μ_s ($J\,mol^{-1}$) of molality m_s ($mol\,kg^{-1}$) by [14]

$$D_{sw} = \frac{u_{+}u_{-}}{Fz_{+}|z_{-}|(\nu_{+}u_{-}+\nu_{-}u_{+})}\frac{\partial\mu_s}{\partial\ln(m_s/m_0)} \tag{18}$$

where m_0 is the reference molal concentration of 1 $mol\,kg^{-1}$. The differential in Eq. (18), per definition of the mean molal activity coefficient of solute s, $\gamma_{\pm}=\gamma_s$, can be re-written as [14]:

$$\frac{\partial\mu_s}{\partial\ln(m_s/m_0)} = RT(\nu_{+}+\nu_{-})\left(1+\frac{\mathrm{d}\ln\gamma_{\pm}}{\mathrm{d}\ln(m_s/m_0)}\right). \tag{19}$$

Finally, incorporating Eqs. (11) and (19) into Eq. (18), we obtain the Nernst–Hartley equation [27]:

$$D_{sw} = \frac{RT}{F^2}\frac{\lambda^{\circ}_{+}\lambda^{\circ}_{-}(\nu_{+}+\nu_{-})}{z_{+}\nu_{+}(\lambda^{\circ}_{+}|z_{-}|+\lambda^{\circ}_{-}z_{+})}\alpha_s \tag{20}$$

where

$$\alpha_s = 1+\frac{\mathrm{d}\ln\gamma_{\pm}}{\mathrm{d}\ln(m_s/m_0)} \tag{21}$$

is the thermodynamic correction factor.

In the limit of infinite dilution, the differential in Eq. (21) tends to zero and we recover Eq. (17). It only remains to verify whether the expression

$$\frac{\lambda^{\circ}_{+}\lambda^{\circ}_{-}(\nu_{+}+\nu_{-})}{z_{+}\nu_{+}(\lambda^{\circ}_{+}|z_{-}|+\lambda^{\circ}_{-}z_{+})} \tag{22}$$

may be treated as independent of concentration. In fact, Robinson and Stokes [14] discussed this problem extensively and showed that the mobility of the ions during diffusion depends much less on concentration than the mobility during electrolytic conduction. Eq. (20) agrees with experimental data within 0.5% up to ca. 0.01 $mol\,L^{-1}$ [14] for aqueous 1:1 electrolytes i.e. for still rather diluted solutions with respect to those used in practical devices such as flow batteries.

6.4. From moderately diluted to concentrated solutions

Agar as well as Robinson and Stokes [14,41] provided an extension of Eq. (20) to take into account additional effects influencing the process of diffusion at extremely high concentrations of >1 $mol\,L^{-1}$:

$$\begin{aligned} D_{sw} = D^{\circ}_{sw}\alpha_s\left(1-0.018hm_s\right)\cdot \\ \left[1+0.018m_s\left([\nu_{+}+\nu_{-}]\frac{D^{*}_{H_2O}}{D^{\circ}_{sw}}-h\right)\right]\frac{\eta_{H_2O}}{\eta} \end{aligned} \tag{23}$$

where h is the solute hydration number, $D^{*}_{H_2O}$ is the self-diffusion coefficient of water estimated to $2.44\cdot10^{-5}$ $cm^2\,s^{-1}$ at 25 °C [14] and the ratio η/η_{H_2O} (the so-called relative dynamic viscosity) is the dynamic viscosity of the electrolyte (Pa s) divided by the dynamic viscosity of the solvent — pure water. It is particularly convenient that all quantities except h in Eq. (23) may be calculated from tabulated limiting mobilities and thermodynamic data.

In Fig. 1(b) we plot experimental ambipolar diffusion coefficient of aqueous HBr and NaBr solutions obtained using a porous-diaphragm method [16]. To test the validity of Eq. (23), we also plot model curves in the same figure. In order to evaluate all terms in Eq. (23) for each solute, we source the available experimental data from the following references (all data for 25 °C).

First, we calculate the limiting ambipolar diffusion coefficients using Eq. (17) and literature limiting molar conductivities from [42]: $\lambda^{\circ}_{Br^-}=78.14\cdot10^{-4}$, $\lambda^{\circ}_{H^+}=349.6\cdot10^{-4}$, $\lambda^{\circ}_{Na^+}=50.08\cdot10^{-4}$, all in $S\,m^2\,mol^{-1}$. The corresponding ambipolar diffusion coefficients at infinite dilution are: $D^{\circ}_{HBr}=3.401\cdot10^{-9}$ and $D^{\circ}_{NaBr}=1.625\cdot10^{-9}$, all in $m^2\,s^{-1}$.

We refer the reader to Appendix D in the Supplementary Material (SM) online for the details of estimating the mean molal activity coefficient to calculate the thermodynamic factor α_s as well as for the methods to calculate the relative dynamic viscosity for HBr and NaBr solutions, which we then use in Eq. (23).

The last required parameter in Eq. (23) is the hydration number. Robinson and Stokes [25, pp. 328–331] discussed in detail the issue of determining h for different electrolytes. They concluded that empirical data up to 1 $mol\,L^{-1}$ may be used to estimate h from diffusion experiments. We adopt the following data from table 11.9 in [25]: $h=1.2$ for NaBr and $h=2.3$ for HBr. The validity of the adopted values of h at concentrations of our interest (much exceeding 1 $mol\,L^{-1}$) is doubtful as hydration may change with concentration and other effects due to short-range forces may arise [25]. In Fig. 1(b) we therefore provide the modelling curves with assuming ±10% variation of h from their reference values.

Overall, the agreement of the literature model by Agar with reference diffusion data is highly satisfactory, at least within the range of available data points. For extreme concentrations, the parameter h impacts the result for HBr significantly stronger than for NaBr due to much higher activity of protons, as evidenced in Fig. 1(a). We shall bear the aforementioned uncertainties in mind when interpreting our results in the next sections.

As indicated before, interpreting the diffusion coefficients measured electrochemically require writing theoretical equations for the transport of *single* ions, like in the case of diffusion of ions with an excess of the supporting electrolyte [Eq. (12)]. In such cases, one will encounter a long-recognised issue in electrochemistry regarding splitting the measurable $\gamma_{\pm}$ into individual ionic contributions, i.e. γ_{+} and γ_{-} [43–45].

Therefore, to split $\gamma_{\pm}$, it is necessary to adopt certain convention [46, p. 15], [47]. For our purpose, we select the simple Debye-Hückel convention:

$$\log_{10}\gamma_{+} = |z_{+}/z_{-}|\log_{10}\gamma_{\pm} \tag{24}$$

$$\log_{10}\gamma_{-} = |z_{-}/z_{+}|\log_{10}\gamma_{\pm} \tag{25}$$

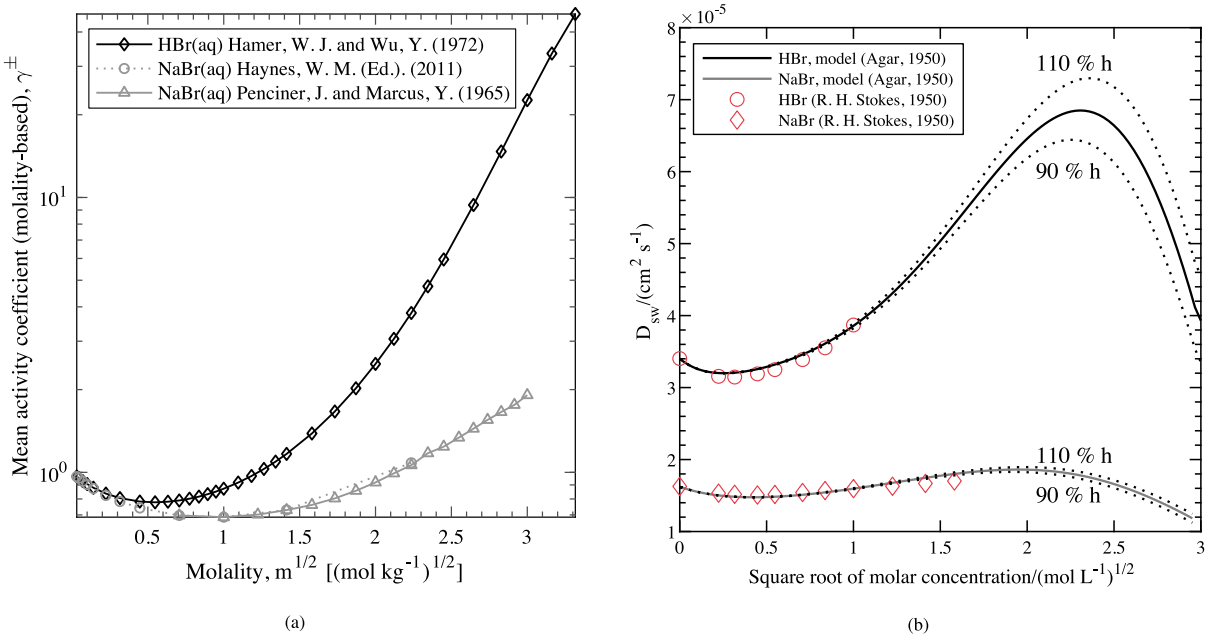

Fig. 1. (a) Mean activity coefficients of aqueous HBr and NaBr solutions at 25 °C. Lines connecting the experimental data points serve as a guide for the eye only; (b) Ambipolar (salt) diffusion coefficient of aqueous HBr and NaBr solutions at 25 °C: experimental data [16] and model by Agar (1950) in: [25].
Source: [42,48,49].

bearing in mind that its usage is questionable beyond 1 $\mathrm{mol\,L^{-1}}$ due to ion hydration effects, as discussed elsewhere [45,46]. It follows that for HBr and NaBr, $\gamma_- \equiv \gamma_\pm$ and thus $\alpha_{\mathrm{Br}^-} \equiv \alpha_s$.

Next, using Eq. (23) written for a "salt", we replace D°_{sw} with $D^\circ_{\mathrm{Br}^-}$, which is the same for both NaBr and HBr:

$$D_{\mathrm{Br}^-} = D^\circ_{\mathrm{Br}^-}\alpha_s\left(1-0.018hm_s\right)\cdot \left[1+0.018m_s\left([\nu_+ + \nu_-]\frac{D^*_{\mathrm{H_2O}}}{D^\circ_{\mathrm{Br}^-}} - h\right)\right]\frac{\eta_{\mathrm{H_2O}}}{\eta}. \quad (26)$$

The other parameters: α, h, η remain dependent on the type of the solute.

6.5. Effect of the electrolyte on limiting currents

The impact of the supporting electrolyte on limiting currents can be quantified by studying the ratio $I_{\mathrm{lim}}/I^{\mathrm{d}}_{\mathrm{lim}}$ where $I^{\mathrm{d}}_{\mathrm{lim}}$ and $I_{\mathrm{lim}} = I^{\mathrm{d}}_{\mathrm{lim}}{}' \pm I^{\mathrm{m}}_{\mathrm{lim}}$ is the limiting current in the presence (diffusion only, d) and absence (diffusion and migration, m) of the supporting electrolyte, respectively. The sign (±) is positive if the two fluxes have the same direction and negative otherwise.

Piatnicki [21] provides an overview of theoretical studies concerning the ratio $I_{\mathrm{lim}}/I^{\mathrm{d}}_{\mathrm{lim}}$. The limiting current due to diffusion at an UME with an excess of supporting electrolyte is [21, p. 28]:

$$I^{\mathrm{d}}_{\mathrm{lim}} = 4nFr_0D^\circ_i c^*_i \quad (27)$$

and in the absence of the supporting electrolyte hypothetically without an external electric field (only concentration gradient, denoted here with a prime):

$$I^{\mathrm{d}}_{\mathrm{lim}}{}' = 4nFr_0D^\circ_{\mathrm{sw}}c^*_s. \quad (28)$$

Eq. (27) is commonly used to estimate diffusion coefficients of ions from the limiting currents at UMEs [22].

For the studies where the transport is resulting from both the diffusional and migrational driving forces due to the external electric field, it is more convenient for modelling to derive expressions for $I_{\mathrm{lim}}/I^{\mathrm{d}}_{\mathrm{lim}}$ on par with formulae for purely diffusional cases, like Eq. (27).

For an electro-oxidation of an anion (here: Br^-) at a UME, Piatnicki [21, p. 29] proposed the following expression for the ratio $I_{\mathrm{lim}}/I^{\mathrm{d}}_{\mathrm{lim}}$:

$$I_{\mathrm{lim}}/I^{\mathrm{d}}_{\mathrm{lim}} = \left(\frac{|z_-|}{z_+}+1\right)\left[\frac{\lambda^\circ_-}{\lambda^\circ_+}\left(1-\frac{n}{|z_-|}\right)+1\right]^{-1}. \quad (29)$$

Plugging in the constants for HBr and NaBr, respectively, into Eq. (29) ($n = 1$), we obtain $I_{\mathrm{lim}}/I^{\mathrm{d}}_{\mathrm{lim}} = 2$. It follows that the limiting current of bromide oxidation without any supporting electrolyte should be *two times higher* than the limiting current predicted by Eq. (27), in which the diffusion coefficient is calculated from Eq. (14). This result agrees exactly with an older theoretical study by Cooper et al. [50] [Table 2 therein, for which the reactant has the charge of $Z = -1$ (Cooper's et al. nomenclature) and the product, bromine, is neutral $z = 0$].

7. Experimental

7.1. Chemical reagents

We used the following reagents directly, without further purification: sodium bromide (NaBr, >99.5%, Sigma), stock hydrobromic acid solution (HBr, 48 wt%, Alfa Aesar), absolute ethanol (EtOH, >99.97%, VWR Chemicals), bromine for synthesis (Br_2, >99.0%, Merck), hexaammineruthenium (III) chloride ($[Ru(NH_3)_6]Cl_3$, >98%, Aldrich), sodium chloride, (KCl, >99.5%, Carl Roth GmbH.), high-purity, oxygen-free, dry argon and nitrogen.

We used ultrapure water (conductivity <0.055 $\mu\mathrm{S\,cm^{-1}}$ at 23 °C) from Purelab Classic machine (ELGA).

7.2. Instrumental

We purchased two working disc ultramicroelectrodes (WE), *002005 MPTE Micro Platinum* and *002007 MCE Micro carbon fibre* (CF) of nominal electrode diameters of 10 μm and 7 μm, respectively, from ALS. A saturated Ag/AgCl electrode (*RE-1B* by ALS) served as reference electrode (RE) and a pure platinum wire as counter electrode (CE). If not stated otherwise, we report all potentials in this paper against this RE.

We polished the working UMEs on a polishing pad (BUEHLER) with diamond polishing pastes MetaDi grades 1 μm and 1/4 μm (BUEHLER) and further refined with diamond polishing suspension MetaDi Supreme grade 0.05 μm (BUEHLER).

The potentiostat used in this study was a VMP3 (Biologic) with low-current option. We controlled the temperature in the electrochemical glass cell (A-001051, Biologic) using a thermostatic bath GD120 (Grant).

7.3. Methods

7.3.1. Main setup

The main experimental setup used for all experiments described herein consisted of a small 20 mL glass cell equipped with a water jacket for precise temperature control at 25, 30, 35 and 40 °C (±0.1 °C).

The cell with a small magnetic stirring bar was positioned above a magnetic stirrer and the whole ensemble was well insulated by wrapping with thermal insulation foam.

The cell was fitted with a polytetrafluoroethylene (PTFE) cap with 4 ports for the WE, RE, CE (three-electrode setup) and a thin glass capillary for argon sparging to remove dissolved oxygen from the electrolyte, and then for maintaining inert gas cushion above the solution (without sparging). The whole cell and equipment was enclosed in a grounded Faraday cage. The current and overpotential conventions employed in this paper follow the IUPAC recommendations (anodic currents and overpotentials have positive signs).

7.3.2. Electrode pre-conditioning and radii determination

We pre-conditionned both UMEs following a polishing procedure with the diamond pastes of gradually decreasing grain size, as described in details in Appendix A in the SM. We determined the radii of both UMEs electrochemically using aqueous solutions of hexaammineruthenium (III) chloride, see Appendix B in the SM for details.

7.3.3. Experiment A: diffusion of bromide in HBr and NaBr solutions

In the Experiment A, we measured mass transport-limited currents at both Pt and CF UMEs in pure HBr and NaBr aqueous solutions in a broad range of concentrations in subsequent dilutions: HBr from the stock solution of 8.852 $\mathrm{mol\,L^{-1}}$ down to 0.0778 $\mathrm{mol\,L^{-1}}$ and NaBr from 6.869 $\mathrm{mol\,L^{-1}}$ to 0.0778 $\mathrm{mol\,L^{-1}}$ (molar concentrations at 25 °C). We analysed HBr solutions at four different temperatures given in Section 7.3.1, whereas NaBr solutions only at 25 °C.

For each solution and both UMEs, we first measured the cell open-circuit voltage (OCV) for 10 s to validate the setup stability. Subsequently, we used a square-wave voltammetry (SWV) technique, scanning the potential of WE from E_i = 0.200 V to E_v = 1.400 V with pulse height of 25.0 mV, pulse width of 50 ms, step height of 10.0 mV and averaging the current over the last 20% of each step, in order to determine the oxidation potential, E_{ox}, at which the diffusion-limited current of bromide oxidation is attained. Experimental details on SWV can be found in Appendix C in the SM.

Next, we performed another OCV hold for 10 s followed by the actual measurement of the limiting currents using a single-step CA. We (1) held the potential of WE at 0.600 V for 10 s, (2) stepped to E_{ox} for 30 s and (3) stepped back to 0.600 V for 30 s. During the second step, we carefully observed the current-time behaviour and inspected if the system reached the steady state (current plateau after the step spike). We show exemplary traces of SWV and CA runs in the results section.

Table 1
Composition of aqueous solutions of HBr with Br_2 used in Experiment B (25 °C).

Solution number	1	2	3	4	5
c^*_{HBr}/(mol L^{-1})	$c^*_{Br_2}$/(mol L^{-1})				
0.1	0.2928	0.1111	0.0555	0.0111	0.0056
0.5	0.7807	0.3027	0.0555	0.0111	0.0056
1.3	2.2445	0.8587	0.0555	0.0111	0.0056
3.5	3.9034	2.2862	0.0555	0.0111	0.0056
6	6.1479	3.9011	0.0555	0.0111	0.0056

7.3.4. Experiment B: diffusion of bromide and bromine in HBr and Br_2 mixtures

In the Experiment B, we determine the mutual impact of bromide and bromine concentrations in aqueous solutions on their diffusion coefficients. We prepared 25 solutions of HBr and Br_2 of various concentrations, as shown in Table 1. The concentrations were selected to cover possibly broad electrolyte composition space without the bromine phase separation, within the minimum limiting currents measurable with the UMEs.

We measured the limiting currents at both Pt and CF UMEs at 25 °C using a single-step CA. The procedure was analogical to the one presented in Section 7.3.3, except here we added an additional CA step to determine the limiting diffusion current of bromine reduction. The potential value of the first step for bromide oxidation (E_{ox}) was determined from SWV as before whereas the potential value for bromine reduction was set constant to E_{red} = 0.250 V. The bromine reduction current was not prone to interference of other reactions as long as the potential was held far more positive with respect to the hydrogen evolution potential. For clarity, we show a typical trace of such experiment in the results section.

8. Results and discussion

8.1. Experiment A: Diffusion of HBr and NaBr in pure aqueous solutions

A typical SWV trace of the net response [51], ΔI (μA), in pure HBr solution of 1.322 $\mathrm{mol\,L^{-1}}$ at Pt and CF UMEs at 25 °C is shown in Fig. 2. We performed the SWV experiment before the CA to determine the potential E_{ox} at which bromide oxidation reaction reaches mass transport limit. The values of E_{ox} were always significantly higher for the CF UME than for the Pt UME due to larger overpotentials of bromide oxidation at carbon materials compared to relatively rapid electrode kinetics at Pt [52].

Aside from the clearly visible Br^- oxidation peak, the experiments with Pt UME revealed additional peaks which are attributed to higher polybromides oxidation (most probably Br_3^-) as well as oxygen evolution at more extreme potentials [19,53,54]. It should be noted that we greatly avoided driving the potential towards oxygen evolution reaction in order not to damage the frangible surface of the UME (especially CF).

In general, E_{ox} decreased with increasing c^*_{HBr} and increasing temperature, which may be explained by the Nernst equation [52]. In the consecutive CA experiment, setting the E_{ox} too high yielded overshot limiting currents due to the additional reactions on top of Br^- oxidation [53]. Too low E_{ox} would result in measurements away from the mass transport limited current regime, in which Eq. (9) is applicable.

Next, for each change in HBr solution concentration and UME, we determined the limiting currents of Br^- oxidation using CA by averaging the plateau currents for 5 s before the potential step end. Examples of chronoamperometric curves are displayed in Fig. 3 for two different concentrations of HBr solutions: 1.322 and 0.438 $\mathrm{mol\,L^{-1}}$ at both CF and Pt UMEs. For Pt UME, we obtained the limiting currents of 0.55 and 0.2 nA and for CF UME: 0.15 and 0.45 nA for the two solutions, respectively.

We note that obtaining limiting currents in unsupported electrolytes at concentrations below ca. 0.08 $\mathrm{mol\,L^{-1}}$ for HBr and ca. 0.16 $\mathrm{mol\,L^{-1}}$

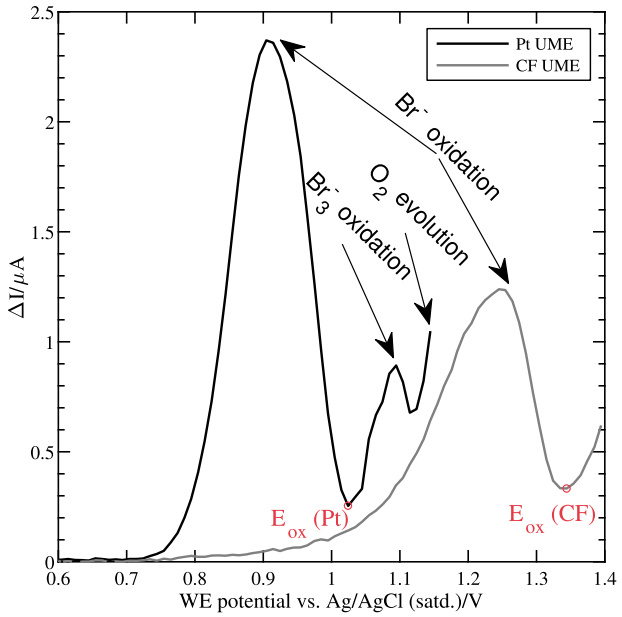

Fig. 2. SWV experiment to determine E_{ox} used in bromide oxidation for the CA experiment. Pure HBr solution of 1.322 mol L^{-1} at Pt and CF UMEs, 25 °C.

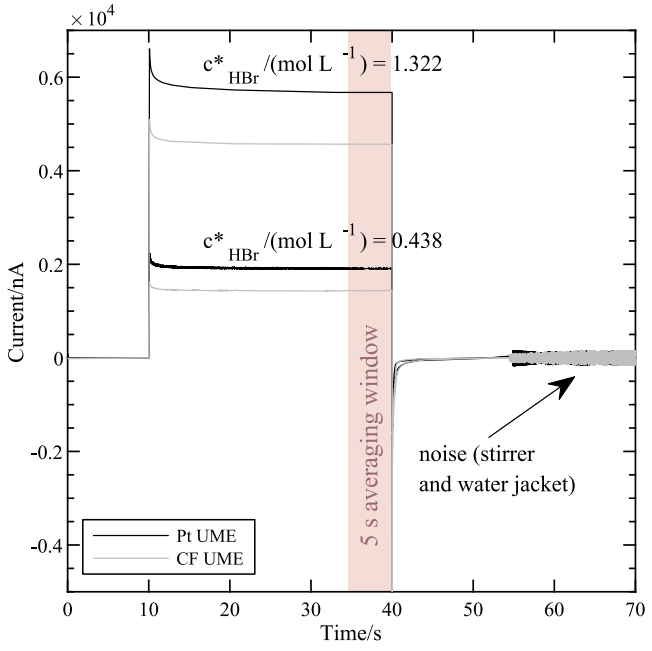

Fig. 3. Chronoamperometric transients of bromide oxidation currents (Experiment A) recorded at Pt and CF UMEs in 1.322 and 0.438 mol L^{-1} HBr at 25 °C. The noise is visible after the stirrer and water flow in the water jacket have been switched back on.

for NaBr was not possible due to poor and distorted signal quality, or no signal at all. The limit is associated with low conductivity of the solutions and low signal-to-noise ratio at low concentrations.

During the measurement, it was crucial to shortly switch off the magnetic stirrer and the flow of water in the water jacket due to a large noise induced by auxiliary electric devices (visible in Fig. 3 at ca. 55 s). The current traces were otherwise stable and controllable, displaying distinct current plateaus shortly after the potential step.

In Fig. 4 we plot the experimental limiting current densities of bromide oxidation calculated as

$$i_{\mathrm{lim}} = \frac{I_{\mathrm{lim}}}{\pi r_0^2} \tag{30}$$

using the CA data of the limiting currents measured in Experiment A for both Pt and CF UMEs at different concentrations of pure HBr and NaBr solutions at 25 °C. We used the data from Table B.7 (SM online) to obtain r_0 for each electrode as well as to calculate the ratio of $R_{\mathrm{el}} = d_0^{\mathrm{Pt}}/d_0^{\mathrm{CF}} = 1.44$.

To facilitate the cross-validation of i_{lim} measured at both electrodes at a given concentration, we additionally divided the respective experimental i_{lim} obtained from the CF UME by R_{el}. By such division, we should obtain very similar limiting current densities results for both Pt and CF UMEs for a broad range of concentrations. The results of such treatment are shown in Fig. 4.

Indeed, for both NaBr and HBr, the i_{lim} measured at the Pt and CF UME agree well with each other within the experimental error. As a matter of fact, the Pt UME had a larger experimental standard deviation, σ_{d_0}, (cf. able B.7 in the SM online), since it is far more prone to trace impurities which led to a larger variance in the electrochemical measurements. This fact appears in Fig. 4 as larger calculated error bars.

The first observation worth commenting is the general non-linearity of the experimental data over the broad range of concentrations, unlike the ubiquitous Eq. (9) with constant D would predict. We analyse this effect further by plotting an apparent diffusion coefficient calculated from the experimental I_{lim} as [cf. Eq. (9)]

$$D^{\mathrm{app}} = \frac{I_{\mathrm{lim}}}{4nFc_s^* r_0} \tag{31}$$

against $\sqrt{c_s}$ for each solute separately. Because the measurements with both Pt and CF UMEs were congruent, in Fig. 5(a) we plot an average of the two D^{app} obtained using the two electrodes for HBr and NaBr at 25 °C.

By and large, D^{app} for low concentrations much below 1 mol L^{-1} decreases sharply with concentration due to the decreasing activity coefficient (cf. Fig. 1(a)). For moderate concentrations, D^{app} increases steadily, mirroring the increase of activity coefficients in this region until reaching a local maximum for very high concentrations. At extremely high concentrations, despite the positive α_{Br^-}, D^{app} decreases again due to the high electrolyte viscosity, hydration and solvent transport effects as discussed previously.

D^{app} of HBr varies much more with concentration than that of NaBr, which is caused by significantly dissimilar activity of both solutes in aqueous solutions. For $\sqrt{c_s} < 0.6$, the measured D^{app} for HBr agrees very well with the result for NaBr. HBr shares a common anion with NaBr and such a result indicates that the we indeed observed the limiting currents due to bromide transport. For higher concentrations, the thermodynamic and transport properties of the two different salts come into play, clearly diversifying the behaviour of the diffusing and migrating bromide species.

For NaBr, the local maximum and then kink downwards of the D^{app} vs. $\sqrt{c_s}$ curve at high concentrations is much more evident than for HBr. Furthermore, certain amount noise is present in the case of HBr at higher concentrations. The reason for this is scrutinised by analysing Fig. 5(b), in which we plot D^{app} vs. $\sqrt{c_s}$ for HBr solely, at different electrolyte temperatures.

For the highest temperature of 40 °C, we confirm the existence of the maximum also for HBr. We seek the explanation of this result in the fact that at high HBr concentration ($c_s > 6$ mol L^{-1}), bromide species are oxidised at the electrode at a relatively high rate, producing elemental bromide which must diffuse away from the electrode surface, causing convective perturbations similar to gas bubbles produced in the case of water electrolysis. At high temperatures, Br_2 dissolves better in the electrolyte and the rate of Br_2 diffusion itself increases, so that

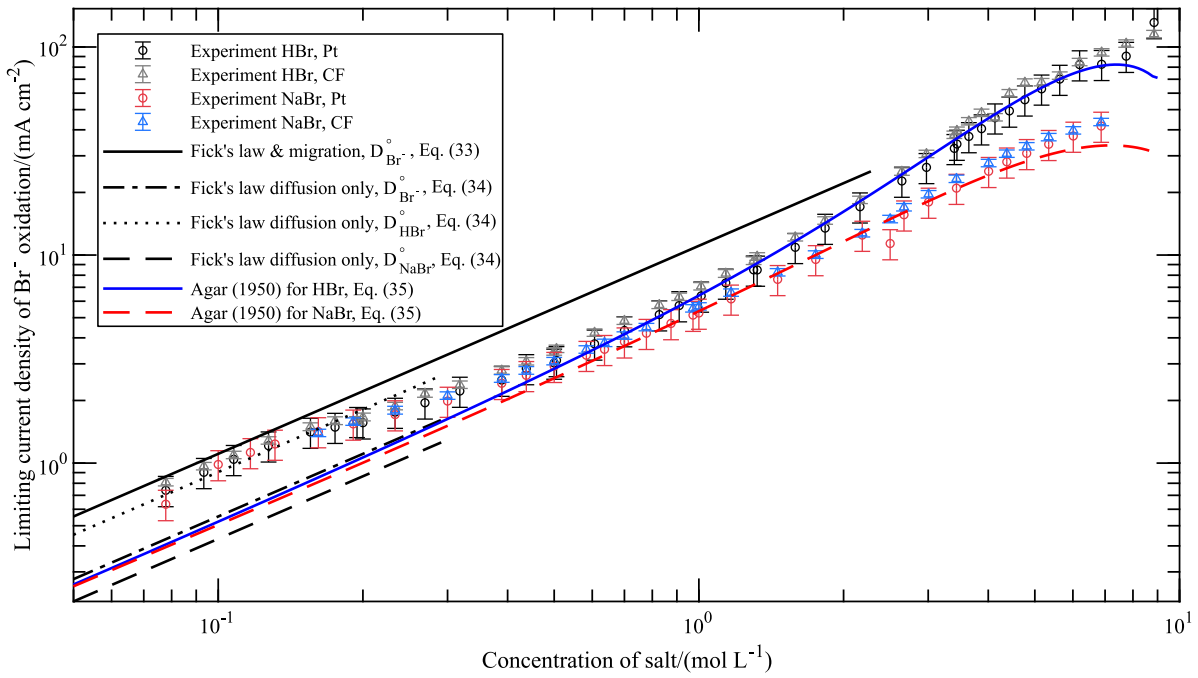

Fig. 4. Limiting current densities of the oxidation of bromide ions in HBr and NaBr solutions (Pt and CF UME experiments) at 25 °C. The modelling curves assuming $D^{\circ}_{Br^-}$ (with and without the migration contribution) and ambipolar diffusion coefficients are plotted for reference. The experimental i_{lim} at CF UME were scaled (divided) by the electrode diameter ratio $R_{el} = 1.44$ to facilitate the comparison with Pt UME results.

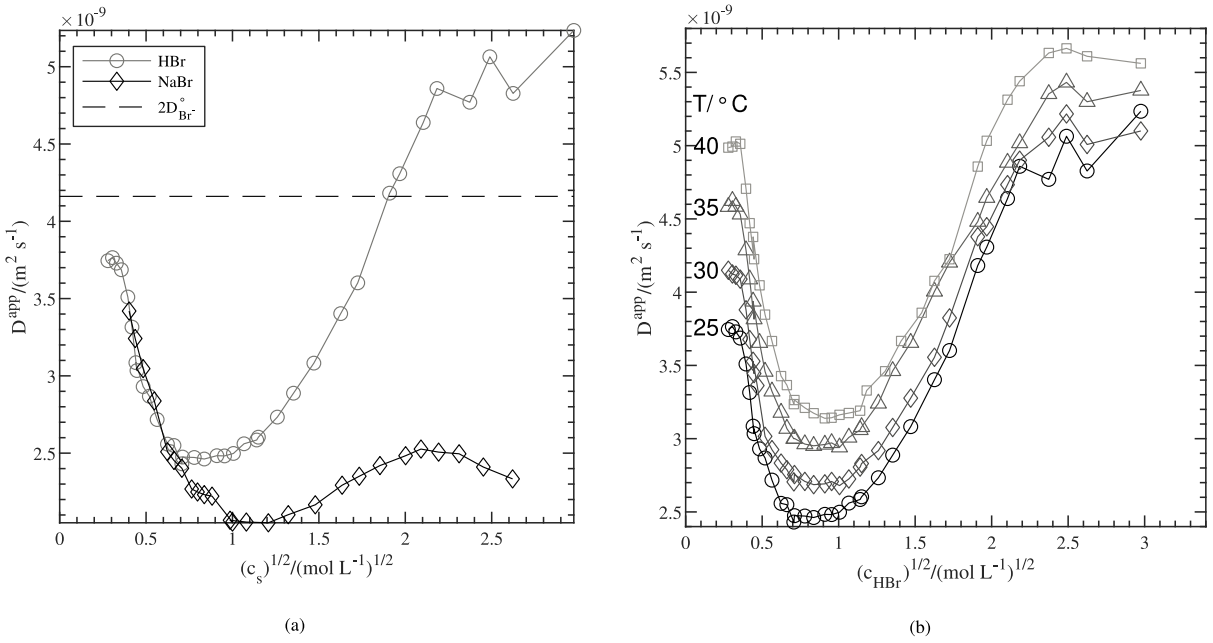

Fig. 5. (a) Apparent diffusion coefficients of bromide anions in HBr and NaBr aqueous solutions (mean from the Pt and CF UME experiments) at 25 °C. The limiting value of $2D^{\circ}_{Br^-}$ (factor of 2 due to migration contribution) is plotted for reference.; (b) Apparent diffusion coefficients of bromide anions in HBr solutions (mean from the Pt and CF UME experiments) at four temperatures between 25 and 40 °C. Lines connecting the experimental data points serve as a guide for the eye only.

it leaves the electrode surface and contributes less to the noise in the current signal, entailing smaller uncertainty and jitter of the measured currents. In general, the Pt UME behaved less stable than CF UME in this concentration region which we justify by a higher catalytic activity of Pt towards bromine reactions than CF [52]. Similar effects due to complexed bromine droplets in the vicinity of the UME was observed previously by Hwang and Chang [18].

To analyse quantitatively the temperature dependence of D^{app} of bromide (mean from Pt and CF UME experiments) in HBr, we select the data for the lowest possible concentration (0.078 mol L^{-1}) and show it as the Arrhenius plot [55, p. 84] in Fig. 6:

$$D^{app} = D^{app}_{\infty} \exp\left(\frac{-E_{a,D}}{RT}\right) \quad (32)$$

where D^{app}_{∞} is the hypothetical apparent diffusion coefficient of species at infinite temperature ($m^2\ s^{-1}$) and $E_{a,D}$ is the diffusional activation energy of the diffusing species (J mol^{-1}). From a linear fit to the four data points for four different temperatures, we obtain $E_{a,D}$ = 14.89 ± 0.32 kJ mol^{-1}. By using Eq. (32) and knowing D^{app}_{∞} at given temperature (e.g. from an isothermal model), one may calculate the

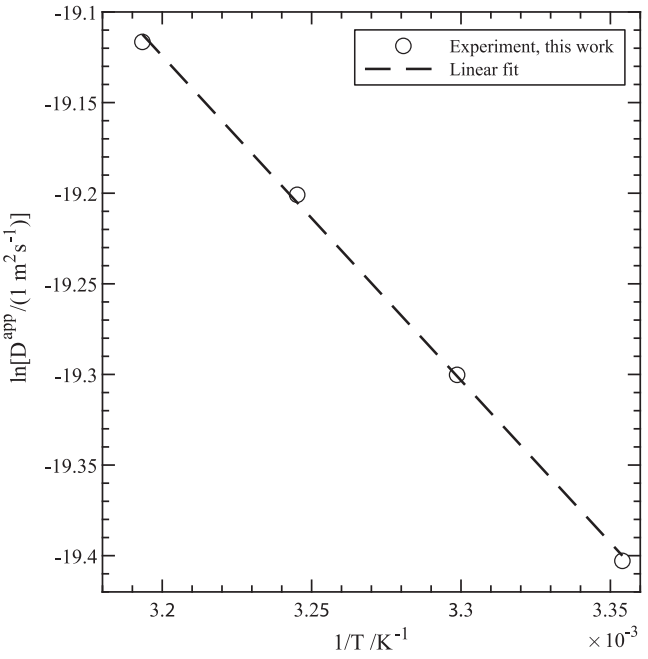

Fig. 6. The temperature dependence of the apparent diffusion coefficient (average from Pt and CF UME experiments) of bromide in 0.078 mol L^{-1} HBr and the resulting linear fit according to the Arrhenius equation.

diffusion coefficient at other temperatures. In the case of HBFB, the typical operating temperatures are in the range of 40 to 50 °C, therefore it is vital to determine the evolution of critical parameters not only with concentration, but also with temperature.

Having expounded qualitatively the experimental peculiarities of UME measurements in pure concentrated HBr and NaBr solutions, we now return to Fig. 4 to interpret quantitatively the obtained results using the available diffusion theory which we introduced earlier in Section 6.

First, we model the limiting current density of bromide ions transport during oxidation at the Pt UME ($n = 1$) assuming no supporting electrolyte, when both migration and diffusion take place, combining Eqs. (9) and (30) into:

$$i_{\mathrm{lim}} = 2\left[4nF D^{\circ}_{\mathrm{Br^-}} c^{*}_{\mathrm{Br^-}} \left(\pi r_0^{\mathrm{Pt}}\right)^{-1}\right]. \tag{33}$$

We plot Eq. (33) vs. solute molarity in Fig. 4 as a black, solid line. Note that for strong electrolytes like HBr, $c^{*}_{\mathrm{Br^-}} = c^{*}_{\mathrm{HBr}}$. According to the discussion in Section 6.5, we multiply the limiting current density by a factor of two in Eq. (33) to account for bromide migration in unsupported HBr and NaBr and use the constant $D^{\circ}_{\mathrm{Br^-}} = 2.081 \cdot 10^{-9}$ $m^2\,s^{-1}$ at 25 °C which we calculated from Eq. (14) using $\lambda^{\circ}_{\mathrm{Br^-}} = 78.14 \cdot 10^{-4}$ $S\,m^2\,mol^{-1}$ [42]. This value was assumed also in HBFB modelling [33,35,36] and electro-analytical chemistry [19,20] papers.

For comparison, in Fig. 4 we also provide a plot (dotted-dashed black line) of the limiting current density of bromide oxidation at Pt UME assuming the presence of excess supporting electrolyte:

$$i^{\mathrm{d}}_{\mathrm{lim}} = 4nF D^{\circ}_{\mathrm{Br^-}} c^{*}_{\mathrm{Br^-}} \left(\pi r_0^{\mathrm{Pt}}\right)^{-1}. \tag{34}$$

Eq. (33) or Eq. (34) with limiting diffusivities are applicable to very diluted solutions (in theory: infinitely diluted), therefore we do not expect them to hold anywhere in the high concentration region.

Eq. (33), i.e. diffusion and migration of bromide without the supporting salt, predicts i_{lim} relatively well in the moderately diluted region. Experimental data for both solutes appear to behave linearly at concentrations lower than 0.15 mol L^{-1} for both solutes. By and large, Eq. (33) seems to slightly overestimate i_{lim} in this region, however 0.1 mol L^{-1} is still far from being an infinitely dilute solution. At even lower concentrations, which are inaccessible with the UME technique without the supporting salt, the apparent $D_{\mathrm{Br^-}}$ is expected to slightly increase (towards the limiting value of $D^{\circ}_{\mathrm{Br^-}}$) and we anticipate the experimental points to approach the theoretical Eq. (33) even closer. This behaviour of D_{app} approaching the infinite dilution limit is also visible in Fig. 5(a), where we plotted $D^{\circ}_{\mathrm{Br^-}}$ (doubled to account for migration) as a dashed line.

In the practical HBFB operating window, we find that for 1 mol L^{-1} HBr, the relative error in limiting current prediction using Eq. (34), used in many theoretical HBFB studies [33,35,36], underestimates the experimental i_{lim} by roughly 50%. On the other hand, for 6 mol L^{-1} HBr, the relative error is +37% and close to zero around 3 mol L^{-1} HBr, which is, however, a pure coincidence.

Investing additional effort in the development of advanced and precise mass transport models for flow batteries yields benefits that extend beyond the realm of pure scientific inquiry. Real HBFB have parallel connections of electrodes, which magnifies the error in predicting an accurate system-level limiting current conditions n-fold, where n is the number of parallel cells in the system. Taking 1 mol L^{-1} HBr as the base case and the associated 50% relative error in i_{lim} estimation and assuming the average limiting current density of 10 mA cm^{-2} with ten parallel cells of 1 m^2 each, the design equations based on regular Fick's law will overestimate the limiting currents by 500 A. This is a considerable difference, impacting the accurate sizing of power electronics.

For the completeness of our arguments, we shall also corroborate the applicability of ambipolar diffusion coefficient of HBr and NaBr to model i_{lim} as expressed in Eq. (28) (diffusion of solute without the supporting electrolyte in the lack of external electric field). To do that, we replace $D^{\circ}_{\mathrm{Br^-}}$ in Eq. (34) with D°_{HBr} or $D^{\circ}_{\mathrm{NaBr}}$, respectively, calculated before in Section 6.4. The simulated curves (dotted and dashed black lines in Fig. 4 respectively) show clearly that although the agreement with experiment for HBr at low concentrations is even better than for Eq. (33), this is only illusory as using the same equation for NaBr yields unsatisfactory results.

We seek clarification of this coincidental agreement for HBr in much higher thermodynamic activity of protons vs. sodium cations at high concentrations. Ultimately, Eq. (34) with ambipolar diffusion coefficients applies to experimental conditions in which the only driving force for transport is the gradient of solute concentration in an unsupported electrolyte, like in the diaphragm method, for example. In the case described in our electrochemical study, the gradient of bromide species and the gradient of the electric potential are present at the same time and this fact most probably invalidates the usage of D°_{sw}.

The next problem to discuss is the departure of the plot i_{lim} vs. c_{s} from linearity at moderate (ca. 1 mol L^{-1}) and high concentrations (>5 mol L^{-1}). To model the i_{lim} in these regions, it is vital to correct the diffusion coefficients as discussed before by using Eq. (23). Using $D^{\circ}_{\mathrm{Br^-}}$ for both solutes with common bromide anion instead of their D°_{sw} and accounting for migration yielded decent agreement of experimental data with the simple theory, at low concentrations. Following this finding, we employ Eq. (26) instead of Eq. (23), which contains single-ion diffusion coefficients, to model the diffusive transport of bromide at higher concentrations, applicable in FB.

At high and moderate electrolyte concentrations, where the electrolyte is present in a large excess, the ion redistribution due to the electron transfer reaction close to the UME surface has little effect on the ionic strength and, therefore, the resistance close to the surface approaches that in the bulk [23,56] and the electrolyte itself may act as a "self-supporting" electrolyte which reduces the influence of migration.

Due to this fact, we use the migration-free Eq. (34):

$$i^{\mathrm{d}}_{\mathrm{lim}} = 4nF D_{\mathrm{Br^-}} c^{*}_{\mathrm{Br^-}} \left(\pi r_0^{\mathrm{Pt}}\right)^{-1}, \tag{35}$$

bearing in mind that it should not be valid in the mixed diffusion–migration transport in the moderate concentrations region.

Note that D_{Br^-} varies now with the concentration according to Eq. (26). We plot the two curves of Eq. (35) for HBr and NaBr in Fig. 4. Additionally, for the purpose of plotting the modelling curve on the same abscissa, we converted molality to molarity of each solute using the following expression:

$$c = m\rho/(mM + 1) \tag{36}$$

where ρ (kg m^{-3}) is the solution density estimated using methods described in Appendix D in the SM and M (g mol^{-1}) is the molar mass of the solute.

Overall, given that we sourced all parameters in Eq. (26) independently and only from the already existing literature, the agreement with our new experiment is excellent in the region of high concentrations. For HBr, the discrepancy is lower than for NaBr at extreme concentrations (>5 mol L^{-1}) and it can be explained by the uncertainty of the determination of h, error propagation from the other solution properties, the usage of the Debye-Hückel convention of splitting $\gamma^{\pm}$ for high concentration as well as additional effects not taken into account (e.g. the degree of dissociation which normally decreases with concentration [57]).

According to the theory, we observe differences of bromide diffusion rate in HBr and NaBr at high concentrations. This is in contrast to the low concentration region, in which the two solutes yield very similar i_{lim}. We note a local maximum and then depression of i^d_{lim} for both solutes due to high electrolyte viscosity and ion hydration at the concentration of ca. 7 mol L^{-1}. The maximum for HBr is considerably higher than for NaBr because aqueous HBr has both higher activity and lower viscosity at 7 mol L^{-1} than NaBr. The last experimental data point for HBr at high concentrations does not seem to agree with the predicted curve. As discussed before and visible in Figs. 5(a) and 5(b), the reason for such disparity is related to high reaction rates of bromine formation at the UME which introduce additional uncertainty in the measurement of the limiting currents at high concentrations. Additionally, we recall the modelling uncertainty related to h at high concentration as well as the questionable applicability of Eq. (25).

We observe that the modelling curves calculated with Eq. (26) begin to agree well with the experiment for both solutes at ca. 0.6 mol L^{-1} and higher. Between ca. 0.13 and 0.6 mol L^{-1} neither Eq. (33) (limiting conditions, diluted electrolytes, migration and diffusion) nor Eq. (35) (concentrated electrolytes, diffusion only, migration fully suppressed due to the "self-supporting" electrolyte in excess) are able to capture the experimental results. At the infinite dilution limit (not shown in Fig. 4), Eq. (26) for both solutes approaches Eq. (34), as expected.

We conclude from the above observations that in the intermediate concentration region (0.13 < c_s < 0.6 mol L^{-1}), modelling of i_{lim} for both solutes is particularly difficult as the ion migration, being only partially eliminated, appears to enhance the mass transport of bromide. We also note that the span of this region may differ, depending on the used solute and the amount of the supporting electrolyte, if any. For more quantitative results, a closer look at the transport mechanism is required. However, since FB usually do not operate at these (rather low) concentrations, we conclude that using Eq. (35) still substantially improves the prediction of the limiting current densities with respect to the ubiquitous Eq. (34).

8.2. Experiment B: Diffusion of bromide and bromine in HBr and Br_2 electrolyte mixtures

To determine the limiting currents in electrolyte mixtures of Br_2 and HBr, we performed a CA experiment with two potential steps. An example of such experiment in a solution of 0.8587 mol L^{-1} in Br_2 and 1.3 mol L^{-1} in Br$^-$ at the Pt and CF UMEs, at 25 °C, is shown in Fig. 7. In this study, the anodic (oxidation) currents suffered from certain amount of noise, especially at the Pt UME, due to the presence of dissolved

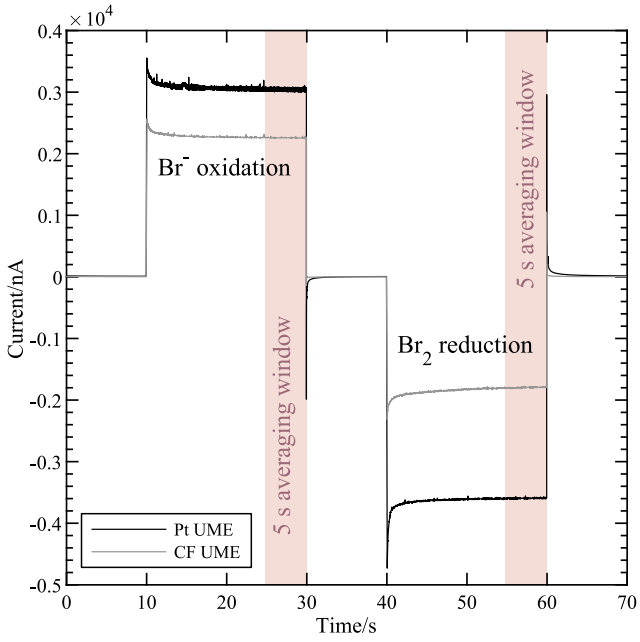

Fig. 7. Chronoamperometric transients of bromide oxidation and bromine reduction currents (Experiment B) recorded at Pt and CF UMEs in a solution of 0.8587 mol L^{-1} in Br_2 and 1.3 mol L^{-1} in HBr at 25 °C.

bromine [58]. This phenomenon (current spikes) is associated with molecular bromine instantaneously adhering to the electrode surface and was studied in detail by Hwang et al. [18] in the context of bromine complexing agents. Despite the noise, we were able to determine the limiting currents by averaging the signal for 5 s before the end of the potential step for each polarisation direction.

The limiting current densities of bromine reduction using the Pt UME at 25 °C for different concentrations of HBr and Br_2 are shown in Fig. 8. In the same figure we also simulate the limiting current density using the simple equation derived from Eq. (27):

$$i^d_{lim} = 4nFD^{\circ}_{Br_2}c^*_{Br_2}\left(\pi r^{Pt}_0\right)^{-1}. \tag{37}$$

Here, we set $n = 2$ and $D^{\circ}_{Br_2} = 1.2 \cdot 10^{-9}$ m^2 s^{-1} which is the literature value of the diffusion coefficient of bromine in water at 25 °C and has been used in HBFB modelling papers [20,33,36] as well as in other papers [19,59].

It is evident from the figure that the common Eq. (37) known from the literature on UMEs with constant $D^{\circ}_{Br_2}$ agrees very well with the experimental results for a very wide range of bromine concentrations. This constancy was also validated in a study by Vogel and Möbius [60]. With increasing Br$^-$ concentration, the diffusion coefficient of bromine apparently increases, enhancing mass transport and thus the current density. This effect, referred to as transfer diffusion [61], is due to the acceleration of transport process in the presence of both reactants undergoing a fast reaction such as Reaction (3) (the "hopping" or Grotthus-like mechanism) [6,62].

Low Br$^-$ concentrations (<0.5 mol L^{-1}) shift the equilibrium Reaction (3) towards reactants (to the left) leaving less polybromides which are needed to enhance the mass transport. Based on the above results we find that Eq. (37) is accurate enough and can be successfully used in most of the HBFB modelling applications, as in FB practice both Br$^-$ and Br_2 are present at high concentrations. At very high Br$^-$ concentrations (>3.5 mol L^{-1}), the limiting current density of bromine reduction appears to be independent of HBr concentration as the experimental data

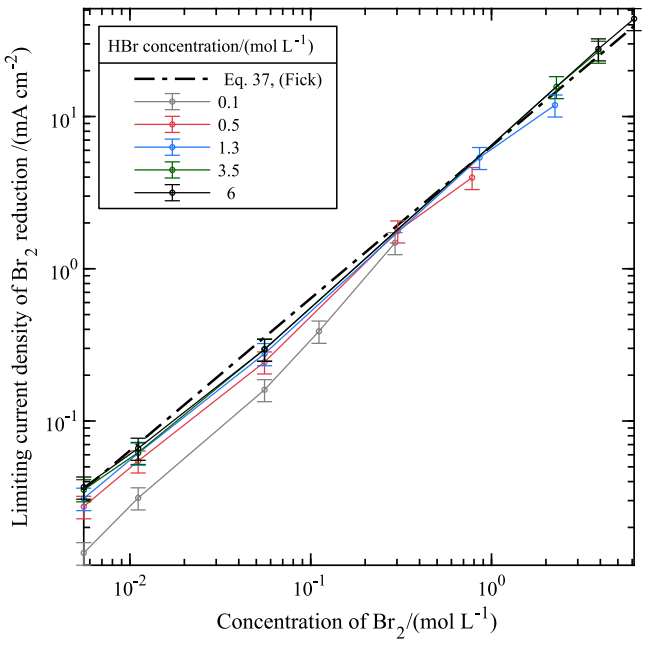

Fig. 8. Diffusion-limited current densities of bromine reduction at different Br_2 and HBr concentration at Pt UME, 25 °C. Lines connecting the experimental data points serve as a guide for the eye only.

points for different Br^- content become essentially indistinguishable. It suggests that at such high HBr concentrations, most of Br_2 is complexed in the form of polybromides.

Contrary to the transport process of charged Br^- species towards the UME, the diffusion of neutral Br_2 appears to comply very well with basic theories such as Fick's law of diffusion [Eq. (37)], even at very high ionic strength.

Next, we analyse the results of limiting current densities of bromide oxidation as a function of HBr and Br_2 concentration at Pt UME, 25 °C. Fig. 9 shows clearly that the rate of mass transport by diffusion and migration of bromide anions towards the electrode significantly decreases with increasing concentration of Br_2. The impact of Br_2 is much more visible for low HBr concentrations (below 3.5 $mol\,L^{-1}$) as the limiting current densities diminish from their approximately constant values (for Br_2-free solutions) starting from relatively low Br_2 concentrations (already for ca. 0.1 $mol\,L^{-1}$ of Br_2 in 0.1 $mol\,L^{-1}$ HBr and for as high as 4 $mol\,L^{-1}$ of Br_2 in 6.0 $mol\,L^{-1}$ HBr).

The above observations allow us to associate the diminution of the limiting current densities of bromide oxidation with the formation of polybromides. When the solution is richer in HBr, more Br_2 is needed to trap bromide anions into complexes and polybromides, such as Br_3^-, are characterised by significantly lower limiting molar ionic conductivities than Br^- alone ($\lambda^\circ_{Br^-}/\lambda^\circ_{Br_3^-} \cong 1.82$ [63]). Polybromides diffuse slower than bromide due to steric effects (i.e. larger hydrodynamic radius as compared to Br^-) [6].

For quantitative results, we model the transport of bromide anions using Eq. (33) in which we multiply the purely diffusive current by two to account for migration, as discussed previously. We plot (dashed lines in Fig. 9) the constant limiting current densities for each HBr concentration resulting from Eq. (33).

For low HBr concentrations (below 0.1 $mol\,L^{-1}$), Eq. (33) predicts the limiting current densities very accurately if the concentration of bromine is not too high to form large amount of polybromides, as discussed previously. For higher HBr concentrations but still within moderate Br_2 concentrations, the simple Eq. (33) largely overestimates the measured limiting current densities and the relative error is the largest (up to ca. −100%) between 0.5 and 1.3 $mol\,L^{-1}$ in HBr. For high Br_2 concentration in the same HBr concentration range, the error is even larger. At very high HBr concentrations (above 6 $mol\,L^{-1}$), the experimental data match again the simple theory for a broad range of Br_2 concentration.

The described diminution of limiting current densities of bromide oxidation at moderate HBr concentrations (between 0.5 and 1.3 $mol\,L^{-1}$) can be explained by two different mechanisms. First, as evidenced from Fig. 1(a) and expounded in Section 6.3, at low to moderate HBr concentrations, the activity coefficient of HBr decreases. This effect impacts the apparent diffusion coefficients measured at UMEs, as evidenced by Figs. 5(a) and 5(b). Secondly, the aforementioned formation of polybromides on addition of substantial amounts of elemental Br_2 reduces the mobility of ions, impacting the diffusion coefficient and drastically decreasing the observed limiting current densities in Fig. 9.

At very high HBr concentrations, the thermodynamic activity of HBr increases and the activity coefficient may attain large values, as we discussed in Section 6.3. Due to this fact, the diffusion coefficient (and thus the limiting current) of HBr increases and at ca. 3.7 $mol\,L^{-1}$ even surpasses the limiting value for infinite dilution, as shown previously in Fig. 5(a). This observation explains why the resulting limiting current density for 6 $mol\,L^{-1}$ in Fig. 9 matches again well with the one predicted by Eq. (33) and corresponds well with the results in Fig. 4. This apparent agreement at high concentrations is, however, just a coincidence mainly resulting from an extremely high activity of HBr compared to that of NaBr. Again, as discussed in Section 8.1, such accordance for NaBr in the region above 4 $mol\,L^{-1}$ would not be the case (cf. Fig. 4).

9. Summary and outlook

In this paper, we showed how UMEs can be leveraged to efficiently measure diffusion and migration-controlled limiting currents in extremely concentrated electrolytes employed in e.g. electrolysers or flow batteries.

Overall, the UME method allowed us to measure limiting currents of bromide oxidation and bromine reduction for a very broad concentration range, spanning three orders of magnitude and for different temperatures. We therefore highly encourage experimental researchers to use UMEs as an inexpensive method to study mass-transport phenomena and to validate mass transport models. Our methodology can be applied to study diffusion in other FB chemistries and diverse electrochemical reactors and electrolysers with concentrated electrolytes.

Br^- transport in pure HBr or NaBr solutions as well as in Br_2–HBr mixtures occurs by means of both diffusion and migration, with various concentration-dependent shares of both transport modes. Below 0.1 $mol\,L^{-1}$ in Br^-, bromide mass transport can be reliably modelled with Fick's law, but must be corrected for migration, because the migration limiting current constitutes 50% of the total measured limiting current.

Between ca. 0.13 and 0.6 $mol\,L^{-1}$, the migration process appears to be only partially suppressed due to higher electrolyte concentration and predicting of Br^- oxidation currents is particularly challenging. Between 0.5 and 1.3 $mol\,L^{-1}$, the experimental limiting currents depend highly non-linearly on bromide concentration and are inferior to those predicted by Fick's law due to low ionic activity and the reduced migration mass flux.

Above 0.6 $mol\,L^{-1}$ in HBr, the transport of Br^- is much enhanced due to high activity of HBr, which is not the case for NaBr. Here, the model of Agar for single-ion diffusion (Br^-) performs remarkably well for both solutes since the migration is seems to be significantly suppressed due to the "self-screening" effect of the concentrated electrolyte. Such effects are to be expected also for other electrolytes in many electrochemical devices. Successful modelling of the transport of uncharged species, like Br_2, requires much less effort than charged species, like Br^- or polybromides.

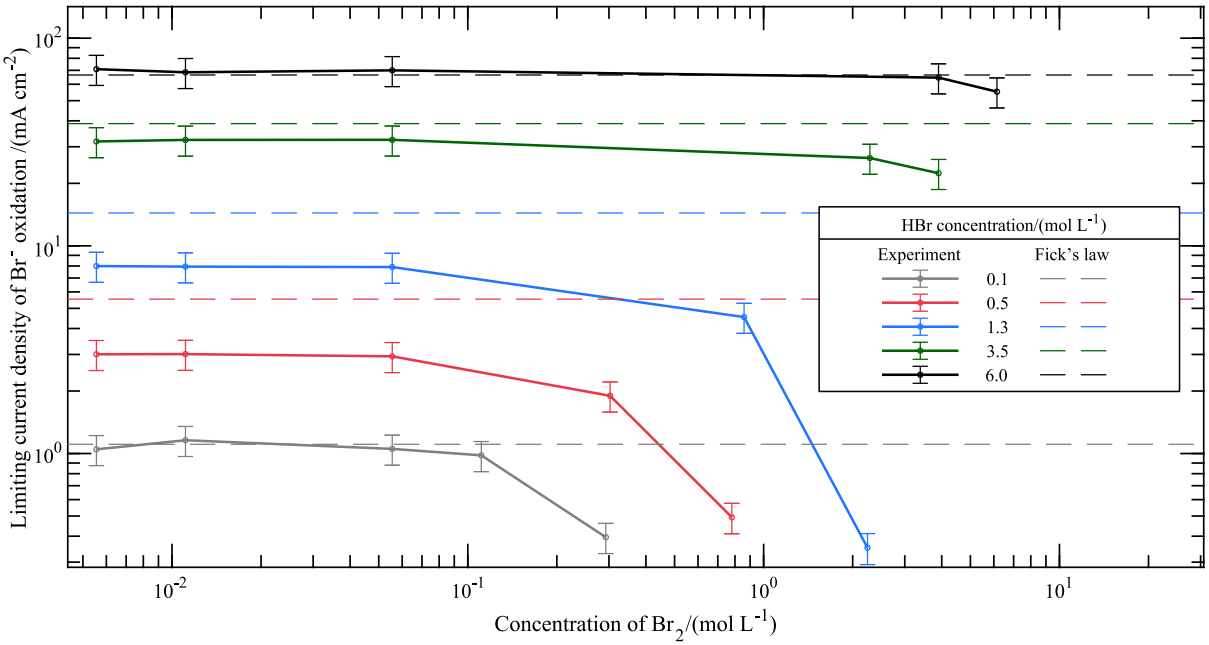

Fig. 9. Limiting current densities of bromide oxidation at different Br_2 and HBr concentration at Pt UME, 25 °C. For reference, dashed lines resulting from Fick's diffusion model with migration [Eq. (33)] are provided. Lines connecting the experimental data points serve as a guide for the eye only.

From the practical perspective, operating the flow battery at concentrations above 3 $\mathrm{mol\,L^{-1}}$ enhances bromide diffusion up to 37% and increases energy density, while at concentrations between 0.3–3 $\mathrm{mol\,L^{-1}}$, diffusion of bromide occurs up to 50% slower with respect to the standard Fick's law predictions. This suggests that there may be a deterioration of flow battery performance due to mass transport resistance in the latter concentration range. Our study also shows that the transport rate of bromine is not concentration-dependent within the concentration ranges typically used in practical flow battery systems (e.g. 3 $\mathrm{mol\,L^{-1}}$ HBr, 1 $\mathrm{mol\,L^{-1}}$ Br2 at state of charge 100%), but excessive bromine concentration close to the solubility limit can substantially hinder the transport of bromide, negatively impacting the charging process. Overall, we provided deep insights into the transport behaviour of bromide and bromine in a HBFB, which can in practice better inform the design and operation of these systems, should more accurate models or digital twins be sought.

Our findings highlight the criticality of leveraging sophisticated mass transport models for accurate design optimisation, as neglecting their significance could lead to substantial over- or underpredictions of parallelised FB cell performance. However, developing these models demands a nontrivial investment of effort and resources that may not always be justified, especially in cases where rough battery sizing estimates are sufficient or if the state of charge of the battery remains fairly constant during operation.

The elucidation of the precise mechanism of bromide species transport within the concentration range of ca. 0.13 to 0.6 $\mathrm{mol\,L^{-1}}$ in Br^- remains an unresolved issue. The extent of ion migration suppression is uncertain, presenting a notable challenge in accurately modelling the limiting currents. Furthermore, additional research is necessary to determine the extent to which the diffusion and migration processes to and from the flat UME surface resemble those occurring within actual porous electrodes, such as carbon felts, papers, woven materials, and membrane-electrode assemblies.

A natural progression of this work is the extension of the UME method to other electrolytes, in particular applied to organic FB electrolytes of low ionic conductivity or bromine-based systems such as Zn-Br with added bromine complexing agents. Based on our developed methods, UMEs may also be implemented as complementary sensors to measure e.g. state of charge of the FB or constitute a valuable source of additional data for battery management systems and online system monitoring, as investigated in recent papers [64,65].

We hope that our contribution pushes forward the limit of understanding transport processes in concentrated electrolytes and harsh, corrosive environments which are omnipresent in the real-world electrochemical applications.

Glossary

Table of acronyms	
Acronym	Explanation
CA	Chronoamperometry
CE	Counter electrode
CF	Carbon fibre
CV	Cyclic voltammetry
EDL	Electric double layer
FB	Flow battery
HBFB	Hydrogen–bromine flow battery
IUPAC	International Union of Pure and Applied Chemistry
NMR	Nuclear Magnetic Resonance
OCP	Open-circuit potential
OCV	Open-circuit voltage
PTFE	Polytetrafluoroethylene
QBr	Quaternary ammonium bromide
RDE	Rotating disc electrode
RE	Reference electrode
SM	Supplementary Material (online)
SWV	Square-wave voltammetry
UME	Ultramicroelectrode
WE	Working electrode

Table of Latin symbols		
Symbol	Explanation	Units/value
a_i	Thermodynamic activity of species i	–
a	Electrode geometry factor	m
A	Electrode surface area	m^2
c_i	Molar concentration of species i	$mol\,L^{-1}$
d_0	Microdisk electrode diameter	m
D_i	Fickian diffusion coefficient of species i	$m^2\,s^{-1}$
D_i°	Single-ion fickian diffusion coefficient of species i at infinite dilution in i and at infinitely small concentration of the supporting salt	$m^2\,s^{-1}$
$D_i^{\circ\prime}$	Single-ion fickian diffusion coefficient of species i at infinite dilution in i and at finite concentration of the supporting salt	$m^2\,s^{-1}$
D_{sw}°	Ambipolar ("salt") diffusion coefficient of salt in water at infinite dilution of the salt	$m^2\,s^{-1}$
$D_{H_2O}^*$	Self-diffusion coefficient of water	$m^2\,s^{-1}$
E	Electric potential	V
$E_{a,D}$	Diffusional activation energy of the diffusing species	$J\,mol^{-1}$
E_i	Initial scanning potential	V
E_v	Final (vertex) scanning potential	V
F	Faraday constant	96 485 $C\,mol^{-1}$
h	Hydration number	–
I	Electric current	A
i_{lim}	Limiting current density	$A\,m^{-2}$
I_{lim}	Limiting current	A
I_{st}	Ionic strength	$mol\,L^{-1}$
ΔI	Net response in SVW experiment	μA
J_i	Molar flux of species i	$mol\,s^{-1}\,m^{-2}$
K_3, K_5, K_7	Equilibrium constant of tri-, penta-, heptabromides formation	–
M	Molar mass of the solute	$g\,mol^{-1}$
m_i	Molality of species i	$mol\,kg^{-1}$
n	Number of electrons transferred	–
N	Number of species in the solution	–
r	Radial space coordinate	m
R	Universal gas constant	$8.314\,J\,K^{-1}\,mol^{-1}$
r_0	Microdisk electrode radius	m
R_{el}	Ratio of Pt and CF UME diameters	–
r_s	Spherical electrode radius	m
t	Time	s
T	Absolute temperature	K
u_i	Ionic mobility of species i	$m^2\,s^{-1}\,V^{-1}$
x	Spatial coordinate	m
z_i	Valence of species i	–

Table of Greek symbols		
Symbol	Explanation	Units
α	Empirical constant in Eq. (13)	–
α_s	Thermodynamic correction factor of salt s	–
η	Dynamic viscosity	Pa s
γ	Activity coefficient on the molal scale	–
λ_i	Molar ionic conductivity of species i	$cm^2\,S\,mol^{-1}$
Λ	Molar ionic conductivity of the electrolyte	$cm^2\,S\,mol^{-1}$
μ_s	Chemical potential of the solute (salt)	$J\,mol^{-1}$
ν_i	Stoichiometric coefficient of the ionic species i	–
ρ	Solution density	$kg\,m^{-3}$
σ	Standard deviation	Depends on the quantity

Table of superscripts	
Symbol	Refers to
*	In the bulk
app	Apparent
∘	In the limit of infinite dilution
d	Diffusion current only
F	Free (uncomplexed)
T	Total

Table of subscripts	
Symbol	Refers to
0	Standard (reference) conditions
±	Mean ionic quantity
+, −	Cations, anions
i	Species i
lim	Limiting (current)
ox	Oxidation
red	Reduction
s	Salt/solute (not individual ionic species)
∞	At the infinite temperature
sw	Salt/solute dissolved in water

CRediT authorship contribution statement

Jakub K. Wlodarczyk: Writing – original draft, Methodology, Conceptualization, Visualization, Investigation, Software. **Norman Baltes:** Writing – review & editing, Conceptualization, Supervision. **K. Andreas Friedrich:** Writing – review & editing, Supervision. **Jürgen O. Schumacher:** Writing – review & editing, Supervision, Funding acquisition.

Declaration of competing interest

The authors declare that they have no known competing financial interests or personal relationships that could have appeared to influence the work reported in this paper.

Data availability

Data will be made available on request

Acknowledgments

This project has received funding from the European Union's Horizon 2020 research and innovation programme under the Maria Skłodowska-Curie Grant Agreement (project "FlowCamp") no. 765289.

The authors kindly acknowledge the contribution of Brenda Berenice Martinez Cantú and Birgit Kintzel from Fraunhofer ICT for their help with tackling technical challenges at the laboratory. We thank Michael Küttinger for providing valuable feedback and proofreading the paper. We are grateful to Dr. Peter Fischer for organisation, managing administrative issues, and making the ICT laboratory available to us.

The experiments described in this paper were conducted from January through March 2021 during the SARS-CoV-2 pandemic.

Appendix A. Supplementary data

Supplementary material related to this article can be found online at https://doi.org/10.1016/j.electacta.2023.142640.

References

[1] H. Zhang, W. Lu, X. Li, Progress and perspectives of flow battery technologies, Electrochem. Energy Rev. 2 (3) (2019) 492–506, http://dx.doi.org/10.1007/s41918-019-00047-1.

[2] O.C. Esan, X. Shi, Z. Pan, X. Huo, L. An, T. Zhao, Modeling and simulation of flow batteries, Adv. Energy Mater. (2020) 2000758, http://dx.doi.org/10.1002/aenm.202000758.

[3] A.C. Ince, C.O. Colpan, A. Hagen, M.F. Serincan, Modeling and simulation of Power-to-X systems: A review, Fuel 304 (2021) 121354, http://dx.doi.org/10.1016/j.fuel.2021.121354.

[4] F.F. Rivera, T. Pérez, L.F. Castañeda, J.L. Nava, Mathematical modeling and simulation of electrochemical reactors: A critical review, Chem. Eng. Sci. 239 (2021) 116622, http://dx.doi.org/10.1016/j.ces.2021.116622.

[5] Y.A. Hugo, W. Kout, G. Dalessi, A. Forner-Cuenca, Z. Borneman, K. Nijmeijer, Techno-economic analysis of a kilo-watt scale hydrogen-bromine flow battery system for sustainable energy storage, Processes 8 (11) (2020) 1492, http://dx.doi.org/10.3390/pr8111492.

[6] M. Küttinger, J.K. Wlodarczyk, D. Daubner, P. Fischer, J. Tübke, High energy density electrolytes for H2/Br2 redox flow batteries, their polybromide composition and influence on battery cycling limits, RSC Adv. 11 (9) (2021) 5218–5229, http://dx.doi.org/10.1039/D0RA10721B.

[7] J.K. Wlodarczyk, M. Küttinger, A.K. Friedrich, J.O. Schumacher, Exploring the thermodynamics of the bromine electrode in concentrated solutions for improved parametrisation of hydrogen–bromine flow battery models, J. Power Sources (2021) 230202, http://dx.doi.org/10.1016/j.jpowsour.2021.230202.

[8] K.T. Cho, P. Ridgway, A.Z. Weber, S. Haussener, V. Battaglia, V. Srinivasan, High performance hydrogen/bromine redox flow battery for grid-scale energy storage, J. Electrochem. Soc. 159 (11) (2012) A1806–A1815, http://dx.doi.org/10.1149/2.018211jes.

[9] M. Küttinger, R. Brunetaud, J.K. Włodarczyk, P. Fischer, J. Tübke, Cycle behaviour of hydrogen bromine redox flow battery cells with bromine complexing agents, J. Power Sources 495 (2021) 229820, http://dx.doi.org/10.1016/j.jpowsour.2021.229820.

[10] M. Küttinger, R. Riasse, J. Wlodarczyk, P. Fischer, J. Tübke, Improvement of safe bromine electrolytes and their cell performance in H2/Br2 flow batteries caused by tuning the bromine complexation equilibrium, J. Power Sources 520 (2022) 230804, http://dx.doi.org/10.1016/j.jpowsour.2021.230804.

[11] R.W. Ramette, D.A. Palmer, Thermodynamics of tri- and pentabromide anions in aqueous solution, J. Solut. Chem. 15 (5) (1986) 387–395, http://dx.doi.org/10.1007/BF00646261.

[12] G. Jones, S. Baeckström, The standard potential of the bromine electrode, J. Am. Chem. Soc. 56 (7) (1934) 1524–1528, http://dx.doi.org/10.1021/ja01322a022.

[13] R.O. Griffith, A. McKeown, A.G. Winn, The bromine-bromide-tribromide equilibrium, Trans. Faraday Soc. 28 (1932) 101–107, http://dx.doi.org/10.1039/TF9322800101.

[14] R.A. Robinson, R.H. Stokes, Electrolyte Solutions, second ed., Dover Publications, Mineola, NY, 2002.

[15] W. Hyk, A. Nowicka, Z. Stojek, Direct determination of diffusion coefficients of substrate and product by chronoamperometric techniques at microelectrodes for any level of ionic support, Anal. Chem. 74 (1) (2002) 149–157, http://dx.doi.org/10.1021/ac0109117.

[16] R.H. Stokes, The diffusion coefficients of eight uni-univalent electrolytes in aqueous solution at 25°c, J. Am. Chem. Soc. 72 (5) (1950) 2243–2247, http://dx.doi.org/10.1021/ja01161a101.

[17] J.K. Klassen, Z. Hu, L.R. Williams, Diffusion coefficients for HCl and HBr in 30 wt % to 72 wt % sulfuric acid at temperatures between 220 and 300 K, J. Geophys. Res.: Atmos. 103 (D13) (1998) 16197–16202, http://dx.doi.org/10.1029/98JD01252.

[18] J. Hwang, J. Chang, Understanding the mass-transfer of Br species in an aqueous and quaternary ammonium polybromide biphasic system via particle-impact electrochemical analysis, J. Ind. Eng. Chem. 80 (2019) 535–544, http://dx.doi.org/10.1016/j.jiec.2019.08.028.

[19] H. Chen, A. Kaliyaraj Selva Kumar, H. Le, R.G. Compton, Non-unity stoichiometric reversible electrode reactions. The effect of coupled kinetics and the oxidation of bromide, J. Electroanal. Soc. 876 (2020) 114730, http://dx.doi.org/10.1016/j.jelechem.2020.114730.

[20] R.E. White, S.E. Lorimer, A model of the bromine/bromide electrode reaction at a rotating disk electrode, J. Electrochem. Soc. 130 (5) (1983) 1096–1103, http://dx.doi.org/10.1149/1.2119890.

[21] C.M.S. Piatnicki, Electrochimie Analytique en Absence d'Electrolyte Indifferent. Transports de Matiere Lors de la Reduction des Acides a une Ultramicroelectrode (Ph.D. thesis), Universite de Nancy, Nancy, 1993.

[22] J. Heinze, Ultramicroelectrodes in electrochemistry, Angew. Chem. Int. Ed. Engl. 32 (9) (1993) 1268–1288, http://dx.doi.org/10.1002/anie.199312681.

[23] I. Montenegro, M.A. Queirós, J.L. Daschbach (Eds.), Microelectrodes: Theory and Applications, 1991st ed., Springer, 2012.

[24] A.J. Bard, L.R. Faulkner, Electrochemical Methods: Fundamentals and Applications, second ed., John Wiley & Sons, 2000.

[25] R.A. Robinson, R.H. Stokes, Electrolyte Solutions, second ed., Dover Publications, Mineola, NY, 2002.

[26] L. Onsager, R.M. Fuoss, Irreversible processes in electrolytes. Diffusion, conductance and viscous flow in arbitrary mixtures of strong electrolytes, J. Phys. Chem. 36 (11) (1932) 2689–2778, http://dx.doi.org/10.1021/j150341a001.

[27] H.J. Tyrrell, K.R. Harris, Diffusion in Liquids, A Theoretical and Experimental Study, Butterworth Publishers, Stoneham, MA, United States, 1984.

[28] D. Miller, Estimation of Tracer Diffusion Coefficients of Ions in Aqueous Solution, Tech. Rep. UCRL-53319, 6860099, 1982, http://dx.doi.org/10.2172/6860099.

[29] B. Huskinson, M.J. Aziz, Performance model of a regenerative hydrogen bromine fuel cell for grid- scale energy storage, Energy Sci. Technol. (2013) 16.

[30] C.A.P. Muñoz, H.H. Dewage, V. Yufit, N.P. Brandon, A unit cell model of a regenerative hydrogen-vanadium fuel cell, J. Electrochem. Soc. 164 (14) (2017) F1717–F1732, http://dx.doi.org/10.1149/2.1431714jes.

[31] Y. Chen, Z. Xu, C. Wang, J. Bao, B. Koeppel, L. Yan, P. Gao, W. Wang, Analytical modeling for redox flow battery design, J. Power Sources 482 (2021) http://dx.doi.org/10.1016/j.jpowsour.2020.228817.

[32] T. Thampan, S. Malhotra, H. Tang, R. Datta, Modeling of conductive transport in proton-exchange membranes for fuel cells, J. Electrochem. Soc. 147 (9) (2000) 3242–3250, http://dx.doi.org/10.1149/1.1393890.

[33] V. Yarlagadda, T. Van Nguyen, A 1D mathematical model of a H2/Br2 Fuel Cell, J. Electrochem. Soc. 160 (6) (2013) F535–F547, http://dx.doi.org/10.1149/2.050306jes.

[34] C. Yin, Y. Gao, G. Xie, T. Li, H. Tang, Three dimensional multi-physical modeling study of interdigitated flow field in porous electrode for vanadium redox flow battery, J. Power Sources 438 (2019) 227023, http://dx.doi.org/10.1016/j.jpowsour.2019.227023.

[35] X. You, Q. Ye, T.V. Nguyen, P. Cheng, 2-D model of a H2/Br2 Flow Battery with flow-through positive electrode, J. Electrochem. Soc. 163 (3) (2016) A447–A457, http://dx.doi.org/10.1149/2.0361603jes.

[36] R. Ronen, I. Atlas, M.E. Suss, Theory of flow batteries with fast homogeneous chemical reactions, J. Electrochem. Soc. 165 (16) (2018) A3820–A3827, http://dx.doi.org/10.1149/2.0251816jes.

[37] R.F. Savinell, S.D. Fritts, Theoretical performance of a hydrogen-bromine rechargeable SPE fuel cell, J. Power Sources 22 (3) (1988) 423–440, http://dx.doi.org/10.1016/0378-7753(88)80035-1.

[38] J. Newman, K.E. Thomas-Alyea, Electrochemical Systems, 3rd Edition, third ed., Wiley-Interscience, Hoboken, N.J, 2004.

[39] A. Gupta, S. Shim, L. Issah, C. McKenzie, H. A. Stone, Diffusion of multiple electrolytes cannot be treated independently: Model predictions with experimental validation, Soft Matter 15 (48) (2019) 9965–9973, http://dx.doi.org/10.1039/C9SM01780A.

[40] B. Balu, A. S. Khair, Role of Stefan–Maxwell fluxes in the dynamics of concentrated electrolytes, Soft Matter 14 (41) (2018) 8267–8275, http://dx.doi.org/10.1039/C8SM01222A.

[41] A.R. Gordon, The diffusion constant of an electrolyte, and its relation to concentration, J. Chem. Phys. 5 (7) (1937) 522–526, http://dx.doi.org/10.1063/1.1750069.

[42] W.M. Haynes (Ed.), CRC Handbook of Chemistry and Physics, ninety-second ed., CRC Press, Boca Raton, Fla., 2011.

[43] R.H. Stokes, R.A. Robinson, Ionic hydration and activity in electrolyte solutions, J. Am. Chem. Soc. 70 (5) (1948) 1870–1878, http://dx.doi.org/10.1021/ja01185a065.

[44] R.G. Bates, Ion activity scales for use with selective ion-sensitive electrodes, Pure Appl. Chem. 36 (4) (1973) 407–420, http://dx.doi.org/10.1351/pac197336040407.

[45] R.G. Bates, B.R. Staples, R.A. Robinson, Ionic hydration and single ion activities in unassociated chlorides at high ionic strengths, Anal. Chem. 42 (8) (1970) 867–871, http://dx.doi.org/10.1021/ac60290a006.
[46] W.E. Morf, The Principles of Ion-Selective Electrodes and of Membrane Transport, Elsevier Science, 2012.
[47] K. Kontturi, L. Murtomäki, J.A. Manzanares, Ionic Transport Processes: In Electrochemistry and Membrane Science, OUP, Oxford, 2008.
[48] W.J. Hamer, Y.-C. Wu, Osmotic coefficients and mean activity coefficients of uni-univalent electrolytes in water at 25 °C, J. Phys. Chem. Ref. Data 1 (4) (1972) 1047–1100, http://dx.doi.org/10.1063/1.3253108.
[49] J. Penciner, Y. Marcus, Activity coefficients of sodium bromide at high concentrations, J. Chem. Eng. Data 10 (2) (1965) 105–106, http://dx.doi.org/10.1021/je60025a006.
[50] J.B. Cooper, A.M. Bond, K.B. Oldham, Microelectrode studies without supporting electrolyte: Model and experimental comparison for singly and multiply charged ions, J. Electroanal. Soc. 331 (1) (1992) 877–895, http://dx.doi.org/10.1016/0022-0728(92)85012-R.
[51] V. Mirceski, S. Komorsky-Lovric, M. Lovric, Square-Wave Voltammetry: Theory and Application, Berlin; London, 2010.
[52] G.H. Schuetz, P.J. Fiebelmann, Electrolysis of hydrobromic acid, Int. J. Hydrogen Energy 5 (3) (1980) 305–316, http://dx.doi.org/10.1016/0360-3199(80)90074-9.
[53] T. Iwasita, M.C. Giordano, Kinetics of the bromine-tribromide-bromide redox processes on platinum electrodes in acetonitrile solutions, Electrochim. Acta 14 (10) (1969) 1045–1059, http://dx.doi.org/10.1016/0013-4686(69)85038-3.
[54] S. Ferro, A.D. Battisti, The bromine electrode. Part I: Adsorption phenomena at polycrystalline platinum electrodes, J. Appl. Electrochem. 34 (10) (2004) 981–987, http://dx.doi.org/10.1023/B:JACH.0000042666.25746.e6.
[55] R.G. Compton, C.E. Banks, Understanding Voltammetry, WSPC, New Jersey, 2018.
[56] K.B. Oldham, Theory of microelectrode voltammetry with little electrolyte, J. Electroanal. Chem. Interfacial Electrochem. 250 (1) (1988) 1–21, http://dx.doi.org/10.1016/0022-0728(88)80189-X.
[57] Y. Marcus, Ionic dissociation of aqueous hydrobromic acid. Part 1.—Estimate from vapour pressure and activity coefficient data, J. Chem. Soc. Faraday Trans. 1 75 (1979) 1715–1727, http://dx.doi.org/10.1039/F19797501715.
[58] M. Goor-Dar, N. Travitsky, E. Peled, Study of hydrogen redox reactions on platinum nanoparticles in concentrated HBr solutions, J. Power Sources 197 (2012) 111–115, http://dx.doi.org/10.1016/j.jpowsour.2011.09.044.
[59] P.K. Adanuvor, R.E. White, S.E. Lorimer, Modeling the rotating disk electrode for studying the kinetics of electrochemical reactions, J. Electrochem. Soc. 134 (3) (1987) 625–631, http://dx.doi.org/10.1149/1.2100519.
[60] I. Vogel, A. Möbius, On some problems of the zinc—bromine system as an electric energy storage system of higher efficiency—I. Kinetics of the bromine electrode, Electrochim. Acta 36 (9) (1991) 1403–1408, http://dx.doi.org/10.1016/0013-4686(91)85326-3.
[61] I. Ruff, V.J. Friedrich, Transfer diffusion. I. Theoretical, J. Phys. Chem. 75 (21) (1971) 3297–3302, http://dx.doi.org/10.1021/j100690a016.
[62] M. Küttinger, P.A. Loichet Torres, E. Meyer, P. Fischer, Properties of bromine fused salts based on quaternary ammonium molecules and their relevance for use in a hydrogen bromine redox flow battery, Chem. – Eur. J. 28 (13) (2022) e202103491, http://dx.doi.org/10.1002/chem.202103491.
[63] J.A. Dean, Lange's Handbook of Chemistry, fifteenth ed., McGraw-Hill Professional, New York, NY, 1998.
[64] B. Segel, Z. Parr, T.V. Sawant, C.S. Yim, D.M. Miller, T.J. Henry, J.R. McKone, Flow battery electroanalysis 3: Online kinetics measurements using ultramicroelectrodes in channel flow, J. Mater. Chem. A (2022) http://dx.doi.org/10.1039/D2TA02132C.
[65] A. Clemente, R. Costa-Castelló, Redox flow batteries: A literature review oriented to automatic control, Energies 13 (17) (2020) 4514, http://dx.doi.org/10.3390/en13174514.